Transient optical response of cold Rydberg atoms with electromagnetically induced transparency

Ya-Wei Guo,[1] Si-Liu Xu,[1,2,*] Jun-Rong He,[1] Pan Deng,[1] Milivoj R. Belić,[3] and Yuan Zhao[4]
[1]*School of Electronic and Information Engineering, Hubei University of Science and Technology, Xianning 437100, China*
[2]*Hubei Institute of Intelligent Mechanical and Electrical Industry Technology, Xianning, 437100, China*
[3]*Texas A&M University at Qatar, P.O. Box 23874 Doha, Qatar*
and Institute of Physics Belgrade, Pregrevica 118, 11080 Zemun, Serbia
[4]*School of Biomedical Engineering, Hubei University of Science and Technology, Xianning 437100, China*

(Received 5 September 2019; accepted 8 January 2020; published 5 February 2020)

We investigate the linear and nonlinear optical response to an optical pumping of a four-level atomic system with electromagnetically induced transparency (EIT) in a cold Rydberg atomic gas. It is found that the transient behavior (especially, the third- and fifth-order susceptibilities) of the probe field, and the steady-state EIT spectrum of the gas, depend crucially on the Rydberg atoms' interaction. Furthermore, we find that the response speed of the Rydberg interaction with EIT can be as much as six times faster than the EIT without the Rydberg interaction, and that the nonlinear response time of the fifth-order optical susceptibility is longer than that of the third-order susceptibility. It is established that the Rydberg blockade effect plays a significant role in increasing the response speed of the Rydberg with EIT.

DOI: 10.1103/PhysRevA.101.023806

I. INTRODUCTION

In the past few decades, huge effort has been directed toward the investigation of electromagnetically induced transparency (EIT) in cold atomic gases [1,2]. Generally, light propagation in media under EIT possesses many interesting properties, such as the reduction of group velocity and the enhancement of Kerr nonlinearity [1–3]. EIT has been utilized for a number of crucial applications, for example, in optical clocks, quantum memory, four-wave mixing, and slow light [4–9]. Nevertheless, the large Kerr nonlinearity found in conventional EIT media [10] is impossible to obtain in nonlinear optics at the single-photon level [11].

In the last two decades, intense research has been undertaken on cold Rydberg atomic gases [12–15], operating in an ultracold environment. Important early theoretical and experimental studies have been performed by Friedler *et al.* [16] and Mohapatra *et al.* [17]. Owing to their interesting properties, including long lifetimes [18], large electric-dipole moments [15], and strong atom-atom interactions (e.g., the Rydberg interaction) [19], Rydberg atoms with EIT have found many important applications, such as direct and nondestructive coherent optical detection [18], precision spectroscopy and measurements [20], quantum computing and information [21], design of devices in quantum information processing [22–24], simulation and manipulation of quantum many-body states [14], and the development of quantum nonlinear optics in correlated quantum many-body systems [25,26].

On the other hand, the study of the nonlinear optical response behaviors, especially the third-order and fifth-order nonlinear optical susceptibilities of the system, is fascinating. Theoretical [27,28] and experimental [29,30] works showed that EIT can be used not only for coherent optical detection of Rydberg atoms, but also for obtaining giant Kerr nonlinearity. Different from conventional EIT media, the giant Kerr nonlinearity in Rydberg-EIT systems comes from the strong Rydberg-Rydberg interaction between atoms, which can be many orders of magnitude larger than those obtained before [31–33]. The third- [31,32] and fifth-order susceptibilities of the probe field in Rydberg-EIT systems [33] have been studied in these works.

It is noticed that most of the studies on Rydberg EIT have been focused on the steady-state or long-time behavior [11,33,34]; the third and fifth order of nonlinear transient optical responses, which develop when the control and the assisted field are turned on, were usually not considered. Nevertheless, in many real considerations, like the performance of quantum devices, the response time of Rydberg EIT is critical. Thus it is necessary to investigate the transient optical response of Rydberg EIT, which is crucial not only for the physical understanding of EIT in Rydberg atoms, but also for real applications of Rydberg-EIT systems [22–24]. Thus, Zhang *et al.* have investigated the transient optical response properties of EIT in a cold Rydberg atomic gas. They found that both the transient behavior and the steady-state EIT spectrum of the three-level atomic system depend strongly on the Rydberg interaction. The response speed of the Rydberg EIT can be five times faster than the conventional EIT without the Rydberg interaction [26].

Before proceeding, we note that this work is different from that in Ref. [26]. Firstly, this four-level system has more tuned parameters. The transient optical response of cold Rydberg atoms depends on the existence of the Rydberg interaction, the control field, and the assisted laser field. Secondly, in our work, the linear and the nonlinear transient behavior of the high-order nonlinear susceptibility of the probe field are demonstrated, and we find that the response speed of the Rydberg interaction with EIT can be six times faster than the EIT without the Rydberg interaction. Thirdly, the stable values of the third-order and the fifth-order nonlinear optical

*xusiliu1968@163.com

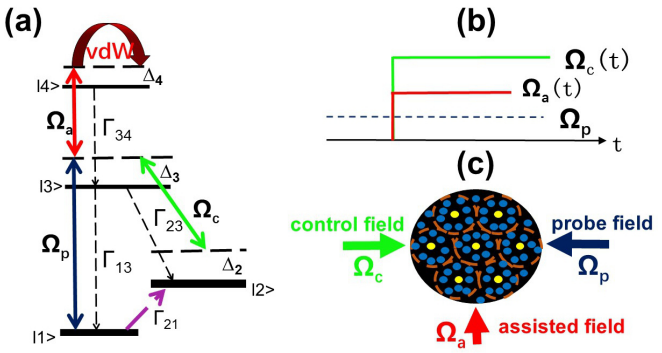

FIG. 1. (a) Level diagram and excitation scheme of the four-level Rydberg-EIT system. States $|1\rangle$, $|2\rangle$, $|3\rangle$ constitute the standard Λ-type EIT configuration, where the probe field (Ω_p) couples the transition $|1\rangle \to |3\rangle$, the control field (Ω_c) couples the transition $|2\rangle \to |3\rangle$, Δ_j are the detunings, and Γ_{jl} are the spontaneous emission decay rates from $|l\rangle$ to $|j\rangle$. The Λ-type EIT is dressed by a high-lying Rydberg state $|4\rangle$, which is far-off-resonantly ($\Delta_3 + \Delta_4 \gg \Omega_a$) coupled to $|3\rangle$ through an assisted laser field E_a (Ω_a). An incoherent population pumping (with pumping rate Γ_{21}) is coupled to $|1\rangle$ and $|2\rangle$, providing a gain for the probe field. (b) Time sequence of the probe (blue dashed line), assistance (red solid line), and the control (green solid line) fields. (c) Schematics of the Rydberg blockade (the orange dashed lines). In each blockade sphere only one Rydberg atom (the small yellow sphere) is excited, and excitations of other atoms (small blue spheres) to their Rydberg states are suppressed.

susceptibilities are displayed. Fourthly, there are more energy-level transition modes in the inverted-Y-type configuration, the control channels are more than lambda-type configuration, and the modulations of energy-level transition are easy to realize, such as the light switch.

The paper is organized as follows. In Sec. II, we describe the four-level atomic model of the Rydberg EIT and introduce the many-atom model. We present analytical results on the transient response by using the reduced density approach. In Sec. III, we display the transient linear and nonlinear optical response of the Rydberg EIT. In Sec. IV, we furnish a summary of the results obtained in this work. The computational details are provided in the Appendixes.

II. MODEL AND MULTIPLE SCALES METHOD

A cold, lifetime-broadened four-level atomic system with an inverted-Y-type configuration is constructed, as shown in Fig. 1(a). The total electric field acting on the atomic system reads as $E = E_p + E_c + E_a$, with $E_v = e_v \varepsilon_v \exp[i(\mathbf{k}_v \cdot r - \omega_v t)]$ (e_v are unit polarization vectors; ε_v are field amplitudes). Here, a weak, spatially focused probe laser field E_p (with the wave number $\mathbf{k}_p = \omega_p/c$, angular frequency ω_p, and half Rabi frequency Ω_p) couples the ground state $|1\rangle$ to the intermediate state $|3\rangle$; a strong control laser field E_c ($\mathbf{k}_c$, ω_c, Ω_c) couples the low-lying state $|2\rangle$ and the state $|3\rangle$. Further, Γ_{13}, Γ_{23}, and Γ_{34} are the spontaneous emission decay rates from $|3\rangle$ to $|1\rangle$, $|3\rangle$ to $|2\rangle$, and $|4\rangle$ to $|3\rangle$, respectively. The states $|1\rangle$, $|2\rangle$, $|3\rangle$, and the probe and control fields constitute a standard Λ-type EIT configuration, which here is dressed by a high-lying Rydberg state $|4\rangle$, being far off resonance through an assisted laser field E_a ($\mathbf{k}_a$, ω_a, Ω_a). In addition, the incoherent population pumping (Γ_{21}) is coupled to the two low-lying states $|1\rangle$ and $|2\rangle$. It may be realized by using several techniques, such as intense atomic resonance spectrum lines emitted from hollow-cathode lamps or from microwave discharge lamps [35]. In our work, a laser-cooled strontium (^{88}Sr) atomic gas is taken as a realistic candidate for our theoretical model described above with $\Gamma_{21} = 0.2\pi \times 10^6\,\mathrm{s}^{-1}$. Here Γ_{21} is an excitation, and it provides a gain, thus suppressing the loss of the probe field. The assigned four atomic levels are $|1\rangle = |5S_{1/2}, F = 1\rangle$, $|2\rangle = |5S_{1/2}, F = 2\rangle$, $|3\rangle = |5, F = 2P_{3/2}, F = 3\rangle$, $|4\rangle = |nS_{1/2}\rangle$. The main quantum number is $n = 60$.

The dynamics of the system is described by the Hamiltonian $\hat{H}_{\mathrm{H}}(t) = N_a \int_{-\infty}^{+\infty} d^3\mathbf{r}\hat{H}_{\mathrm{H}}(\mathbf{r}, t)$, where N_a is the atomic density. Under electric-dipole and rotating-wave approximations, the Hamiltonian density in the interaction picture reads as

$$\begin{aligned}\hat{H}_{\mathrm{H}}(\mathbf{r}, t) = &\sum_{j=1}^{4} \hbar\Delta_j \hat{S}_{jj}(\mathbf{r}, t) - \hbar[\Omega_p \hat{S}_{13}(\mathbf{r}, t) + \Omega_a \hat{S}_{34}(\mathbf{r}, t) \\ &+ \Omega_c \hat{S}_{23}(\mathbf{r}, t) + \mathrm{H.c.}] \\ &+ N_a \int_{\mathbf{r}' \neq \mathbf{r}} d^3\mathbf{r}' \hat{S}_{44}(\mathbf{r}', t)\hbar V(\mathbf{r}' - \mathbf{r})\hat{S}_{44}(\mathbf{r}, t), \end{aligned} \tag{1}$$

where $\hat{S}_{jl} = |l\rangle\langle j| \exp i[(\mathbf{k}_l - \mathbf{k}_j) \cdot \mathbf{r} - (\omega_l - \omega_j + \Delta_l - \Delta_j)t]$ is the transition operator related to the states $|j\rangle$ and $|l\rangle$, satisfying the commutation relation $[\hat{S}_{jl}(\mathbf{r}, t), \hat{S}_{\mu\nu}(\mathbf{r}', t)] = (1/N_a)\delta(\mathbf{r}' - \mathbf{r})[\delta_{j\nu}\hat{S}_{\mu l}(\mathbf{r}', t) - \delta_{\mu l}\hat{S}_{j\nu}(\mathbf{r}', t)]$, with N_a the atom density and $\hbar\omega_j$ the eigenenergy of the level $|j\rangle$; $\Delta_3 = (\omega_3 - \omega_1) - \omega_p$ is the one photon detuning, $\Delta_2 = \omega_p - \omega_c - (\omega_2 - \omega_1)$ and $\Delta_4 = \omega_p + \omega_a - (\omega_4 - \omega_1)$ the two-photon detunings; $\Omega_p = (\mathbf{e}_p \cdot \mathbf{p}_{31})\varepsilon_p/\hbar$, $\Omega_c = (\mathbf{e}_c \cdot \mathbf{p}_{32})\varepsilon_c/\hbar$, and $\Omega_a = (\mathbf{e}_a \cdot \mathbf{p}_{43})\varepsilon_a/\hbar$ are the half Rabi frequencies of the probe, control, and assisted fields, with $\mathbf{p}_{lj}$ being the electric-dipole matrix elements associated with the transition $|l\rangle \to |j\rangle$. The last term in Eq. (1) is the contribution due to atom-atom interaction. The interaction between the Rydberg atom at position $\mathbf{r}$ and the one at position $\mathbf{r}'$ is described by the long-range potential $\hbar V(\mathbf{r} - \mathbf{r}')$, with $V(\mathbf{r} - \mathbf{r}') = C_6/|\mathbf{r}' - \mathbf{r}|^6$. C_6 is the dispersion parameter ($C_6 = -2\pi \times 81.6\,\mathrm{GHz}\,\mu\mathrm{m}^6$). Due to Rydberg interaction, the Rydberg excitation of one atom would block the Rydberg excitation of all surrounding atoms with the blockade sphere radius of R_b [36]; see Fig. 1(c). One can see that the system can be divided into many small blockade spheres, and each blockade sphere contains only one Rydberg atom.

According to the Heisenberg equation of motion for $\hat{S}_{jl}(\mathbf{r}, t)$, one can obtain the equation of the one-body correlators $\rho_{jl}(\mathbf{r}, t) \equiv \langle \hat{S}_{jl}(\mathbf{r}, t)\rangle$:

$$i\frac{\partial}{\partial t}\rho_{11} + i\Gamma_{21}\rho_{11} - i\Gamma_{13}\rho_{33} - \Omega_p\rho_{13} + \Omega_p^*\rho_{31} = 0, \tag{2a}$$

$$i\frac{\partial}{\partial t}\rho_{22} - i\Gamma_{21}\rho_{11} - i\Gamma_{23}\rho_{33} - \Omega_c\rho_{23} + \Omega_c^*\rho_{32} = 0, \tag{2b}$$

$$i\frac{\partial}{\partial t}\rho_{33} + i\Gamma_3\rho_{33} - i\Gamma_{34}\rho_{44} + \Omega_p\rho_{13} - \Omega_{\rm p}^*\rho_{31} + \Omega_c\rho_{23} - \Omega_c^*\rho_{32} - \Omega_a\rho_{34} + \Omega_a^*\rho_{43} = 0, \tag{2c}$$

$$i\frac{\partial}{\partial t}\rho_{44} + i\Gamma_{34}\rho_{44} + \Omega_a\rho_{34} - \Omega_a^*\rho_{43} = 0, \tag{2d}$$

$$\left(i\frac{\partial}{\partial t} + d_{21}\right)\rho_{21} + \Omega_c^*\rho_{31} - \Omega_p\rho_{23} = 0, \tag{2e}$$

$$\left(i\frac{\partial}{\partial t} + d_{31}\right)\rho_{31} + \Omega_p(\rho_{11} - \rho_{33}) + \Omega_c\rho_{21} + \Omega_a^*\rho_{41} = 0, \tag{2f}$$

$$\left(i\frac{\partial}{\partial t} + d_{41}\right)\rho_{41} + \Omega_a\rho_{31} - \Omega_p\rho_{43} - N_a\int d^3\mathbf{r}'V(\mathbf{r}' - \mathbf{r})\rho_{44,41}(\mathbf{r}', \mathbf{r}, t) = 0, \tag{2g}$$

$$\left(i\frac{\partial}{\partial t} + d_{32}\right)\rho_{32} + \Omega_p\rho_{12} + \Omega_c(\rho_{22} - \rho_{33}) + \Omega_a^*\rho_{42} = 0, \tag{2h}$$

$$\left(i\frac{\partial}{\partial t} + d_{42}\right)\rho_{42} + \Omega_a\rho_{32} - \Omega_c\rho_{43} - N_a\int d^3\mathbf{r}'V(\mathbf{r}' - \mathbf{r})\rho_{44,42}(\mathbf{r}', \mathbf{r}, t) = 0, \tag{2i}$$

$$\left(i\frac{\partial}{\partial t} + d_{43}\right)\rho_{43} + \Omega_a(\rho_{33} - \rho_{44}) - \Omega_{\rm p}^*\rho_{41} - \Omega_{\rm c}^*\rho_{42} - N_a\int d^3\mathbf{r}'V(\mathbf{r}' - \mathbf{r})\rho_{44,43}(\mathbf{r}', \mathbf{r}, t) = 0, \tag{2j}$$

where $d_{jl} = \Delta_j - \Delta_l + i\gamma_{jl}$ $(i, j = 1, 2, 3, 4;\ i \neq j)$, and $\gamma_{jl} = (\Gamma_j + \Gamma_l)/2 + \gamma_{ij}^{\rm dep}$ with $\Gamma_l = \sum_{j<l}\Gamma_{jl}$. Here Γ_{jl} denotes the spontaneous emission decay rate from the state of the transition operator to the states $|j\rangle$ and $|l\rangle$, and $\gamma_{ij}^{\rm dep}$ denotes the dephasing rate between the states $|j\rangle$ and $|l\rangle$.

From Eqs. (2a)–(2j), we can see that for solving the equations of motion of the one-body correlators, one needs to know the two-body correlators $\rho_{44,4j}(\mathbf{r}, \mathbf{r}', t) \equiv \langle\hat{S}_{44}(\mathbf{r}, t)\hat{S}_{4j}(\mathbf{r}', t)\rangle$ $(j = 1, 2, 3)$. In the same way, to solve the equations of motion of the two-body correlators, one needs to know the three-body correlators $\rho_{jl,\mu\nu,\xi\eta}(\mathbf{r}, \mathbf{r}', \mathbf{r}'', t) \equiv \langle\hat{S}_{jl}(\mathbf{r}, t)\hat{S}_{\mu\nu}(\mathbf{r}', t)\hat{S}_{\xi\eta}(\mathbf{r}'', t)\rangle$, etc. As a result, one obtains an infinite hierarchy of equations of motion for the correlators of one-body, two-body, three-body, and so on. The equations of motion of the one-body correlators are given by Eqs. (2a)–(2j). Equations of motion of two-body correlators are not listed here, since there are 42 independent equations and each of them is rather long [see Appendix A], with additional three-body correlators and the corresponding spatial integrals. Because these equations are nonlinearly coupled with each other, it is difficult to solve them by using conventional techniques. As the probe-field intensity is relatively small, one can employ the method of reduction perturbation, widely applied in the nonlinear oscillation and wave theory [37], to solve the equations. Because our calculation is exact to fifth order, the equations of motion for the n-body correlators $(n \geqslant 5)$ are not needed [33].

To obtain divergence-free solutions for the one- and two-body correlators of the order of magnitude in the equations for the one-body correlators $\rho_{jl} \equiv \langle\hat{S}_{jl}\rangle$ and the two-body $\rho_{jl,\mu\nu} \equiv \langle\hat{S}_{jl}\hat{S}_{\mu\nu}\rangle$ correlators, we make the following expansions: $\Omega_p = \varepsilon\Omega_p^{(1)}$, $\rho_{j1} = \sum_{m=0}\varepsilon^{2m+1}\rho_{j1}^{(2m+1)}$, $\rho_{jl} = \sum_{m=1}\varepsilon^{2m}\rho_{jl}^{(2m)}$, $\rho_{11} = 1 + \sum_{m=1}\varepsilon^{2m}\rho_{11}^{(2m)}$, $\rho_{j1,l1} = \sum_{m=1}\varepsilon^{2m}\rho_{j1,l1}^{(2m)}$, $\rho_{j1,1l} = \sum_{m=1}\varepsilon^{2m}\rho_{j1,1l}^{(2m)}$, $\rho_{jl,\mu1} = \sum_{m=1}\varepsilon^{2m+1}\rho_{jl,\mu1}^{(2m+1)}$, and $\rho_{jl,\mu\upsilon} = \sum_{m=2}\varepsilon^{2m}\rho_{jl,\mu\upsilon}^{(2m)}$ $(j, l, \mu, \upsilon = 2, 3, 4)$. Here, ε is a small expansion parameter, characterizing the magnitude of the amplitude of the probe-field Rabi frequency. All the quantities on the right-hand side of the expansions given above are considered as functions of the fast time variable $t_0 = t$ and the slow time variable $t_2 = \varepsilon^2 t$ [37,38]. Then, we obtain a set of linear but inhomogeneous differential equations for each of the equations of the one- and two-body correlators, which can be solved analytically order by order up to the fifth-order approximation.

At the first [i.e., $O(\varepsilon)$] order, only the equations for one-body correlators are to be solved. Using the initial condition $\rho_{21}^{(1)}(0) = 0$, $\rho_{31}^{(1)}(0) = -\Omega_p^{(1)}/d_{31}$, $\rho_{41}^{(1)}(0) = 0$, we obtain the solution for $\rho_{j1}^{(1)}$, which exhibits a damped fast oscillation (as a function of t_0) modulated by two envelopes $f_1^{(1)}$ and $f_2^{(1)}$ (as functions of t_2) [see Appendix C]. At the second [i.e., $O(\varepsilon^2)$] order, we obtain the lowest-order solution of the two-body correlators, with the given set of initial conditions $\rho_{31,31}^{(2)}(0) = (\Omega_p^{(1)}/d_{31})^2$, $\rho_{31,13}^{(2)}(0) = |\Omega_p^{(1)}/d_{31}|^2$, and other $\rho_{j1,l1}^{(2)}(0) = \rho_{j1,1l}^{(2)}(0) = 0$. The second-order solution for the one-body correlators $\rho_{jl}^{(2)}$ can also be gained simultaneously with the set of initial conditions $\rho_{33}^{(2)}(0) = 2\gamma_{31}|\Omega_p^{(1)}|^2/(\Gamma_{13}|d_{31}|^2)$ and other $\rho_{jl}^{(2)}(0) = 0$. With these results, one proceeds to the third [i.e., $O(\varepsilon^3)$] -order approximation. Solutions of $\rho_{jl,\mu1}^{(3)}$ and $\rho_{j1}^{(3)}$ at this order are also obtained in Appendix B. A solvability condition used to get the envelopes $f_1^{(1)}$ and $f_2^{(1)}$ appeared in the first-order solution. Steps for obtaining approximate solutions up to the fifth order for the equations of one- and two-body correlators by using the method of multiple scales are described in detail in Appendix B. Because of the complexity involved in the formulas, we will not write the fourth- or fifth-order expansions here.

III. TRANSIENT RESPONSE OF THE RYDBERG EIT

Combining the solutions gained from the first- to the third- and fifth-order approximations described above, and after returning to the original variables, we obtain the transient

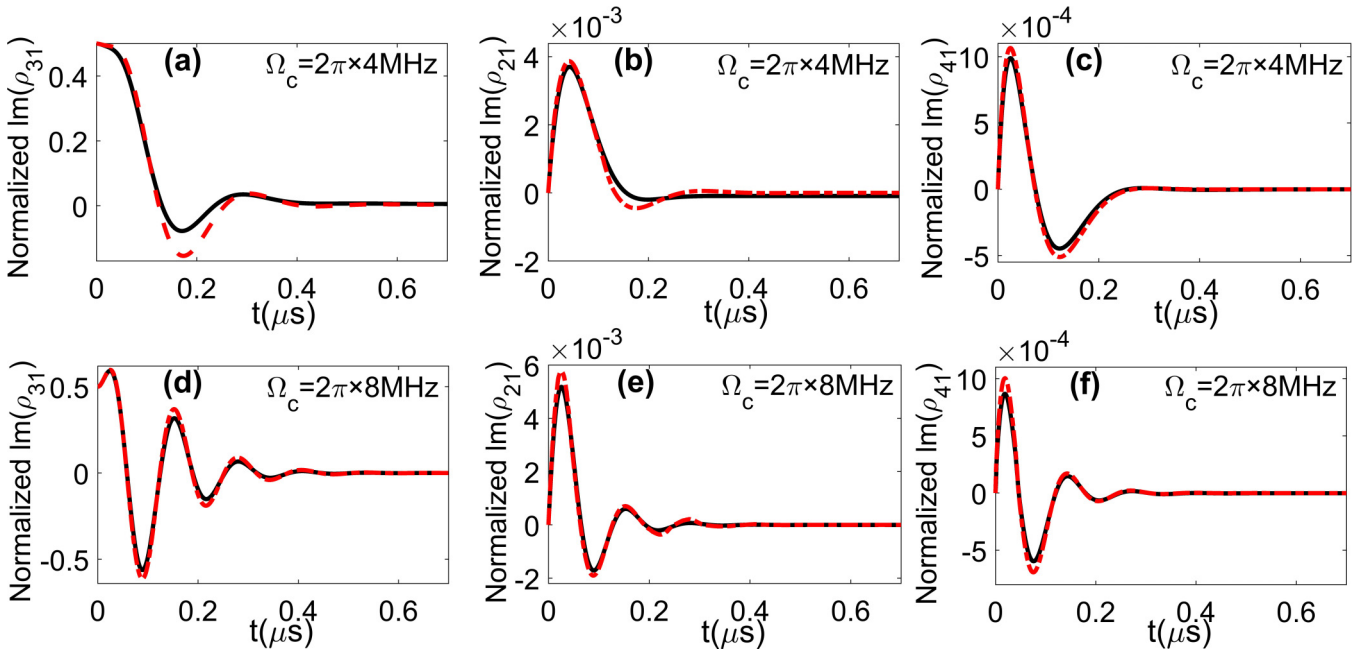

FIG. 2. Transient response of the Rydberg EIT as a function of time t with $\Omega_p = 0.5\Gamma_{13}$ and $\Omega_a = 13\,\mathrm{MHz}$. (a,d) Normalized absorption $\mathrm{Im}(\rho_{31})$. (b,e) Normalized absorption $\mathrm{Im}(\rho_{21})$. (c,f) Normalized absorption $\mathrm{Im}(\rho_{41})$. The black solid line is with Rydberg interaction (i.e., high atomic density $N_a = 1.0 \times 10^{12}\,\mathrm{cm}^{-3}$); the red dotted line is without Rydberg interaction (low atomic density $N_a = 1.0 \times 10^{8}\,\mathrm{cm}^{-3}$). (a–c) $\Omega_c = 2\pi \times 4\,\mathrm{MHz}$; (d–f) $\Omega_c = 2\pi \times 8\,\mathrm{MHz}$. Other parameters are $\Gamma_{21} = 0.2\pi \times 10^6\,\mathrm{s}^{-1}$, $\Gamma_3 = \Gamma_{13} + \Gamma_{23} = 20\pi \times 10^6\,\mathrm{s}^{-1}$, and $\Gamma_4 = \Gamma_{34} \approx 0.0334\pi \times 10^6\,\mathrm{s}^{-1}$.

optical response function of the Rydberg EIT:

$$\rho_{31}(t) \approx a_{31}^{(1)}(t)\Omega_p + \left[a_{31}^{(3),\mathrm{LA}}(t) + N_a \int d^3\mathbf{r}' V(\mathbf{r}' - \mathbf{r}) a_{31}^{(3),\mathrm{RR}} \times (\mathbf{r}' - \mathbf{r}, t)\right]|\Omega_p|^2\Omega_p + \left[a_{31}^{(5),\mathrm{LA}}(t) + N_a \int d^3\mathbf{r}' V(\mathbf{r}' - \mathbf{r}) a_{31}^{(5),\mathrm{RR}}(\mathbf{r}' - \mathbf{r}, t)\right]|\Omega_p|^4\Omega_p. \tag{3}$$

Here, the first term on the right-hand side is the linear description of the complete optical response of the system. The second and third terms are the third order and fifth order nonlinear description of the system, respectively. The nonlinear response includes two parts. One is a nonlocal nonlinear response, described by $N_a \int d^3\mathbf{r}' V(\mathbf{r}' - \mathbf{r}) a_{31}^{(3),\mathrm{RR}}(\mathbf{r}' - \mathbf{r}, t)|\Omega_p|^2\Omega_p + N_a \int d^3\mathbf{r}' V(\mathbf{r}' - \mathbf{r}) a_{31}^{(5),\mathrm{RR}}(\mathbf{r}' - \mathbf{r}, t)|\Omega_p|^4\Omega_p$, which is contributed by the Rydberg interaction; another one is a local nonlinear response, described by the term $a_{31}^{(3),\mathrm{LA}}(t)|\Omega_p|^2\Omega_p + a_{31}^{(5),\mathrm{LA}}(t)|\Omega_p|^4\Omega_p$, which is contributed by the photon-atom interaction (see Appendix B).

In addition, we are interested in the nonlinear optical effects, especially the third-order and fifth-order nonlinear optical susceptibilities of the system. To this aim, we need the relation between the optical susceptibility of the probe field and the density matrix elements. Since the total electric polarization intensity of the system is given by $\mathbf{P} = N_a \sum_{j,l=1}^{4} p_{jl}\rho_{lj} \exp\{i[(\mathbf{k}_l - \mathbf{k}_j)\cdot\mathbf{r} - (\omega_l - \omega_j + \Delta_l - \Delta_j)t]\}$, the electric polarization intensity of the probe field reads as $\mathbf{P}_p = N_a\{p_{13}\rho_{31}\exp[i(\mathbf{k}_p\cdot\mathbf{r} - \omega_p t)] + \mathrm{c.c.}\}$, by which one can obtain the optical susceptibility χ_p of the probe field by using the formula $\mathbf{P}_p = \varepsilon_0\chi_p\mathbf{e}_p\varepsilon_p\exp[i(\mathbf{k}_p\cdot\mathbf{r} - \omega_p t)] + \mathrm{c.c.}$, which yields $\chi_p = \frac{N_a(\mathbf{e}_p\cdot\mathbf{p}_{13})\rho_{31}}{\varepsilon_0\varepsilon_p}$. Collecting the first-order to the fifth-order solutions of ρ_{31} obtained above, we find $\rho_{31} = a_{31}^{(1)}\Omega_p + a_{31}^{(3)}|\Omega_p|^2\Omega_p + a_{31}^{(5)}|\Omega_p|^4\Omega_p + \cdots$, where $\rho_{31}^{(j)}(j = 1, 3, 5, \cdots)$ are independent of Ω_p. Using the formula of susceptibility and the definition $\Omega_p = (\mathbf{e}_p\cdot\mathbf{p}_{31})\varepsilon_p/\hbar$, we have

$$\chi_p = \chi_p^{(1)} + \chi_p^{(3)}|\varepsilon_p|^2 + \chi_p^{(5)}|\varepsilon_p|^4, \tag{4}$$

where $\chi_p^{(1)}$, $\chi_p^{(3)}$, $\chi_p^{(5)}$ are, respectively, the first-order (linear), and the third-order and the fifth-order (nonlinear) optical susceptibilities of the probe field, defined by $\chi_p^{(1)} = N_a|\mathbf{p}_{13}|^2 a_{31}^{(1)}/\varepsilon_0\hbar$, $\chi_p^{(3)} = \chi_{p1}^{(3)} + \chi_{p2}^{(3)}$, $\chi_p^{(5)} = \chi_{p1}^{(5)} + \chi_{p2}^{(5)}$, with $\chi_{p1}^{(3)} = \frac{N_a|\mathbf{p}_{13}|^4}{\varepsilon_0\hbar^3 D_2}[d_{21}d_{41}(a_{33}^{(2)} - a_{11}^{(2)}) - d_{41}\Omega_c a_{23}^{(2)} - d_{21}\Omega_a^* a_{43}^{(2)}]$, $\chi_{p2}^{(3)} = -\frac{N_a^2|\mathbf{p}_{13}|^4\Omega_a^*}{\varepsilon_0\hbar^3 D_2}[d_{21}\int d^3\mathbf{r}' V(\mathbf{r}' - \mathbf{r}) a_{44,41}^{(3)}]$, $\chi_{p1}^{(5)} = \frac{N_a|\mathbf{p}_{13}|^6}{\varepsilon_0\hbar^5 D_2}[d_{21}d_{41}(a_{33}^{(4)} - a_{11}^{(4)}) - d_{41}\Omega_c a_{23}^{(4)} - d_{21}\Omega_a^* a_{43}^{(4)}]$, $\chi_{p2}^{(5)} = -\frac{N_a^2 d_{21}|\mathbf{p}_{13}|^6\Omega_a^*}{\varepsilon_0\hbar^5 D_2}\int d^3\mathbf{r}' V(\mathbf{r}' - \mathbf{r}) a_{44,41}^{(5)}$, with $D_2 = d_{21}d_{31}d_{41} - |\Omega_c|^2 d_{41} - |\Omega_a|^2 d_{21}$, where $\chi_{p1}^{(3)}$ and $\chi_{p1}^{(5)}$ are the third-order and the fifth-order nonlinear optical susceptibilities arising from the interaction between the probe field and the atoms; $\chi_{p2}^{(3)}$ and $\chi_{p2}^{(5)}$ are the third-order and fifth-order nonlinear optical susceptibilities arising from the Rydberg-Rydberg interaction.

Figure 2 shows the normalized absorptions $\mathrm{Im}(\rho_{31})$, $\mathrm{Im}(\rho_{21})$, and $\mathrm{Im}(\rho_{41})$ as a function of t by taking $\Omega_p = 0.5\Gamma_{13}$, $\Omega_a = 13\,\mathrm{MHz}$, $\Gamma_{21} = 0.2\pi \times 10^6\,\mathrm{s}^{-1}$, $\Gamma_3 = \Gamma_{13} + \Gamma_{23} = 20\pi \times 10^6\,\mathrm{s}^{-1}$, $\Gamma_4 = \Gamma_{34} \approx 0.0334\pi \times 10^6\,\mathrm{s}^{-1}$. Here, the normalized absorption coefficient is obtained by

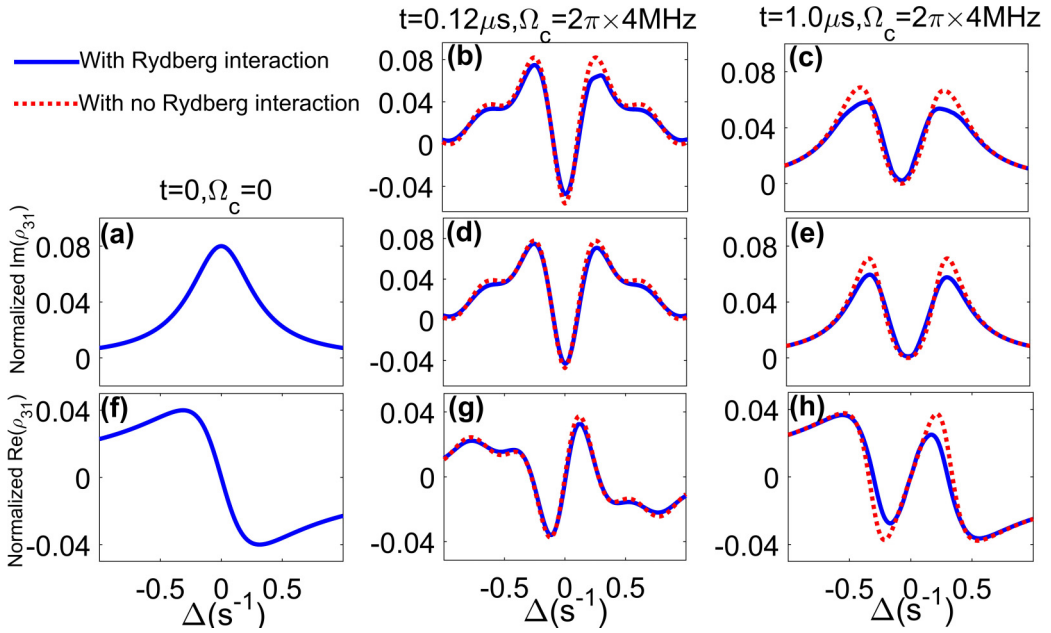

FIG. 3. Transient response behavior of the Rydberg EIT as a function of the probe-field detuning Δ ($\equiv \Delta_2{=}\Delta_3 = \Delta_4$) with $\Omega_p = 0.08\Gamma_{13}$, $\Omega_a = 23$ MHz. (a–e) Normalized absorption spectrum $\mathrm{Im}(\rho_{31})$. (b,c) and (d,e) are without and with the higher-order corrections in Eq. (3), respectively. (f–h) Normalized dispersion spectrum $\mathrm{Re}(\rho_{31})$. The blue solid line is the EIT spectrum with significant Rydberg interaction ($N_a = 1.0 \times 10^{12}\,\mathrm{cm}^{-3}$), and the red dashed line is the EIT spectrum without Rydberg interaction ($N_a = 1.0 \times 10^{8}\,\mathrm{cm}^{-3}$). (a,f) $t = 0$ and $\Omega_c = 0$. (b,d,g) $t = 0.12\,\mu$s and $\Omega_c = 2\pi \times 4$ MHz. (c,e,h) $t = 1.0\,\mu$s and $\Omega_c = 2\pi \times 4$ MHz. Other parameters are the same as in Fig. 2.

dividing the actual absorption coefficient by the absorption peak when the control light is zero [$\mathrm{Im}(\rho_{31})$]. In Figs. 2(a)–2(c), the black solid line is with Rydberg interaction (i.e., high atomic density $N_a = 1.0 \times 10^{12}\,\mathrm{cm}^{-3}$); the red dotted line is without Rydberg interaction (low atomic density $N_a = 1.0 \times 10^{8}\,\mathrm{cm}^{-3}$) for $\Omega_c = 2\pi \times 4$ MHz. Due to the Rydberg interaction, the Rydberg excitation of one atom would block the Rydberg excitation of all surrounding atoms for $R_b \geqslant r_{AB}$, here, $R_b = (C_6/\Delta_{\mathrm{EIT}})^{1/6}$ is the blockade sphere radius [34], $\Delta_{\mathrm{EIT}} = \Omega_c^2/\gamma_{31}$ is the linewidth of the EIT transmission window. $r_{AB} = (5/9)N_a^{-1/3}$ is the average interatomic separation [39]. When $N_a = 1.0 \times 10^{12}\,\mathrm{cm}^{-3}$, $\gamma_{31} = 10\pi$ MHz, and $\Omega_c = 2\pi \times 4$ MHz, one has $R_b \approx 5.42\,\mu$m and $r_{AB} = 0.56\,\mu$m, which satisfies $R_b \geqslant r_{AB}$ for the case with the Rydberg interaction [34,40]. On the other hand, when the system is at low atomic density with $N_a = 1.0 \times 10^{8}\,\mathrm{cm}^{-3}$ and $\Omega_c = 2\pi \times 4$ MHz, one can get $r_{AB} = 12\,\mu\mathrm{m} > R_b$ for the case without the Rydberg interaction. Figures 2(d)–2(f) show the results for a large control field, i.e., $\Omega_c = 2\pi \times 8$ MHz. The time sequence is shown in Fig. 1(b). From Figs. 2(a) and 2(d), one can see, firstly, that both the absorption curves of the EIT with and without the Rydberg interaction present a damped oscillation, before reaching a small steady-state value as the control and the assisted field are switched on. Secondly, the oscillation amplitude for the case with the Rydberg interaction is smaller (the black solid line) compared to the case with no Rydberg interaction (the red dotted line). The transient response time with the Rydberg interaction is faster than that without Rydberg interaction. Thirdly, one can see the transient response time increases with the value of Ω_c for the same atom density. Similar characteristics are displayed in $\mathrm{Im}(\rho_{21})$ [Figs. 2(b) and 2(e)] and $\mathrm{Im}(\rho_{41})$ [Figs. 2(c) and 2(f)]. However, the oscillation amplitudes of $\mathrm{Im}(\rho_{31}) > \mathrm{Im}(\rho_{21}) > \mathrm{Im}(\rho_{41})$. This demonstrates that the atoms nearly remain as their initial states. Hence, the strong Rydberg interaction shifts the Rydberg state out of resonance and then blocks its excitation.

Figures 3(a)–3(e) show the numerical results of normalized absorption spectrum $\mathrm{Im}(\rho_{31})$ as a function of the probe-field detuning Δ ($\equiv \Delta_2{=}\Delta_3 = \Delta_4$) at $\Omega_p = 0.08\Gamma_{13}$ and $\Omega_a = 23$ MHz. Figure 3(a) shows the normalized absorption spectrum $\mathrm{Im}(\rho_{31})$ for $t = 0$ and $\Omega_c = 0$. Figures 3(b)–3(e) show the absorption spectrum without and with inclusion of higher-order correction in Eq. (3). One can see that after the control and the assisted field are switched on, an EIT transparency window opens near $\Delta = 0$. The original single-peak absorption spectrum [Fig. 3(a)] evolves into a structure with two peaks, and the separation between the two peaks is gradually increased as t increases [Figs. 3(b)–3(e)]. The depth of the EIT transparency window for the case of the EIT with the Rydberg interaction (blue solid line) is shallower than that of the EIT without Rydberg interaction (red dashed line) [Figs. 3(b)–3(e)], which means that, comparing with the EIT with no Rydberg interaction, the final steady-state absorption in the EIT with the Rydberg interaction is stronger. The absorption profile in Figs. 3(b) and 3(c) are asymmetric (blue solid lines). When the time evolution increases, we obtain the approximate symmetric two-peak structure [blue solid lines in Figs. 3(d) and 3(e)]. It is shown that the higher-order corrections in Eq. (3) eliminate the asymmetric profiles presented in Fig. 3.

Figures. 3(f)–3(h) show that the dispersion property of the system is described by the real part of the atomic coherence $\mathrm{Re}(\rho_{31})$ as a function of the probe-field detuning Δ ($\equiv \Delta_2{=}\Delta_3 = \Delta_4$) with $\Omega_p = 0.08\Gamma_{13}$ and $\Omega_a = 23$ MHz. One can see that when the control and the assisted field are switched on ($t > 0$) [Fig. 1(b)] in the dispersion spectrum

TABLE I. Response time T_R of the Rydberg EIT for $\Omega_p = 0.2\Gamma_{13}$ and $\Omega_a = 10\,\mathrm{MHz}$.

Ω_c	T_R with Rydberg interaction (high atomic density is $N_a = 1.0 \times 10^{12}\,\mathrm{cm}^{-3}$)	T_R with no Rydberg interaction (low atomic density is $N_a = 1.0 \times 10^{8}\,\mathrm{cm}^{-3}$)
$2\pi \times 4\,\mathrm{MHz}$	$0.24\ \mu\mathrm{s}$	$1.45\ \mu\mathrm{s}$
$2\pi \times 6\,\mathrm{MHz}$	$0.33\ \mu\mathrm{s}$	$1.56\ \mu\mathrm{s}$
$2\pi \times 8\,\mathrm{MHz}$	$0.41\ \mu\mathrm{s}$	$1.67\ \mu\mathrm{s}$

for $t > 0$, an anomalous dispersion [Fig. 3(f)] evolves into a normal dispersion near $\Delta = 0$ [Figs. 3(g) and 3(h)]. Further, when $t = 0.12\,\mu\mathrm{s}$, near $\Delta = 0$, there is almost no difference of the dispersion behavior between the case with (blue solid lines) and without (red dashed lines) the Rydberg interaction [Fig. 3(g)]. If $t = 1.0\,\mu\mathrm{s}$ is chosen, a small difference in the dispersion behavior and a smaller group velocity are displayed in Fig. 3(h). Thus, by using the Rydberg EIT, one can obtain slower group velocity, which is useful for the slowdown and memory of optical pulses.

Based on the above results, one can deduce that the EIT with Rydberg interaction has a faster response time than the EIT without Rydberg interaction. To support this conclusion, we give a qu-antitative estimate on the response time of the Rydberg EIT [40,41] (see Appendix C). Table I shows the response time T_R of the Rydberg EIT for $\Omega_a = 10\,\mathrm{MHz}$ and $\Omega_p = 0.2\Gamma_{13}$ with different control-field values Ω_c; the other parameters are the same as in Fig. 2. Here, T_R is the time of $\mathrm{Im}(\rho_{31})$ reaching steady state. It is shown that for a small control field of $\Omega_c = 2\pi \times 4\,\mathrm{MHz}$, and a high atomic density ($N_a = 1.0 \times 10^{12}\,\mathrm{cm}^{-3}$), the response time of the Rydberg EIT is approximately six times smaller than that of the EIT without Rydberg interaction ($N_a = 1.0 \times 10^{8}\,\mathrm{cm}^{-3}$). The physical reason is due to the Rydberg blockade in the Rydberg-EIT system, where the strong Rydberg interaction shifts the Rydberg state $|4\rangle$ out of resonance and then blocks its excitation. As a result, atoms nearly remain in their initial three-level atomic states; hence the steady-state EIT can be achieved at an early time in the Rydberg system, which is also confirmed in Fig. 2. Further, the larger the value of Ω_c, the longer the response time of EIT. As to the enhancement of the coherence of the system, when Ω_c increases, the oscillation frequency of $\mathrm{Im}(\rho_{31})$ increases as well. Thus, a longer time is needed for $\mathrm{Im}(\rho_{31})$ to evolve into the steady state. This point is clearly seen by the black solid line and the red dashed line in Figs. 2(a) and 2(d).

Figure 4 shows that the response time of the Rydberg EIT [$\mathrm{Im}(\rho_{31})$] can change as the probe and the assistant field Rabi frequencies Ω_p, Ω_a and the average interatomic separation r_{AB} are varied. Figure 4(a) shows the response time T_R [see Fig. (7) in Appendix C] as a function of Ω_p with $\Omega_c = 2\pi \times 4\,\mathrm{MHz}$ and $\Omega_a = 10\,\mathrm{MHz}$. The blue line and the red dotted line are for the cases with the Rydberg interaction and without the Rydberg interaction, respectively. One can see that as $\Omega_p < 0.01\Gamma_{13}$, the response time of the EIT with the Rydberg interaction is almost equal to that of the EIT without the Rydberg interaction. As the probe-field Rabi frequency Ω_p increases, the response time of the EIT with the Rydberg interaction reduces rapidly and it becomes faster than that without the Rydberg interaction. However, the response time of the EIT without the Rydberg interaction goes first down, then up, and finally keeps the same tendency as Ω_p increases. Figure 4(b) shows the response time T_R as a function of Ω_a with $\Omega_c = 2\pi \times 4\,\mathrm{MHz}$ and $\Omega_p = 0.2\Gamma_{13}$. One can see that T_R slowly increases as Ω_a increases both with and without the Rydberg interaction, and T_R with the Rydberg interaction is shorter than that without the Rydberg interaction. The physical reason is mainly due to the Rydberg blockade effect. In each blockade sphere only one atom is excited to the Rydberg state $|4\rangle$; other atoms can be excited only to the state $|3\rangle$. Thus, the Rydberg-EIT system has a larger relaxation rate compared to the EIT system without the Rydberg interaction. As a result, the dissipation of the system is enhanced, giving rise to a decreased response time for the Rydberg-EIT system. Figure 4(c) shows the response time T_R as a function of the average interatomic separation r_{AB} with $\Omega_p = 0.2\Gamma_{13}$ and $\Omega_a = 10\,\mathrm{MHz}$. From Fig. 4(c), it is shown that T_R grows with r_{AB} ($5.42\,\mu\mathrm{m} \leqslant r_{AB} \leqslant 8.2\,\mu\mathrm{m}$). There are two extreme points (dots M and N). When $N_a = 1.1 \times 10^{9}\,\mathrm{cm}^{-3}$ (dot M, $r_{AB} = 5.42\,\mu\mathrm{m}$), $\Omega_c = 2\pi \times 4\,\mathrm{MHz}$, and $\gamma_{31} = 10\pi\,\mathrm{MHz}$, one can get $T_R = 0.24\,\mu\mathrm{s}$ and $R_b{=}r_{AB}$, where the Rydberg excitation tends to saturate. This is due to

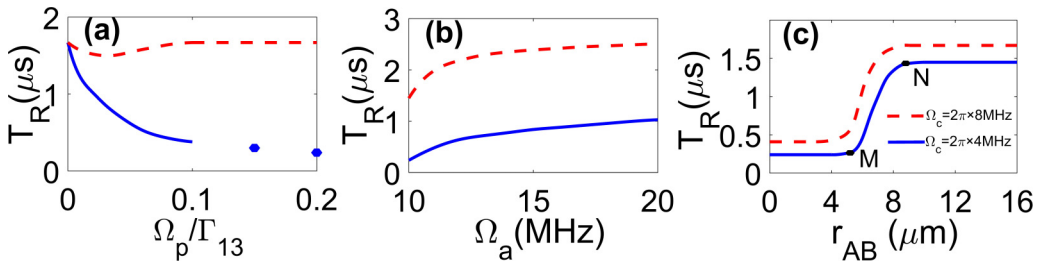

FIG. 4. (a) Response time T_R of the EIT as a function of the probe-field Rabi frequency Ω_p with the Rydberg interaction (blue solid line) and without the Rydberg interaction (red dotted line) for $\Omega_c = 2\pi \times 4\,\mathrm{MHz}$ and $\Omega_a = 10\,\mathrm{MHz}$. (b) Response time T_R of the EIT as a function of the assisted field Rabi frequency Ω_a with the Rydberg interaction (blue) and with no Rydberg interaction (red dotted) for $\Omega_p = 0.2\Gamma_{13}$ and $\Omega_c = 2\pi \times 4\,\mathrm{MHz}$. (c) The response time T_R of the Rydberg EIT vs r_{AB} for $\Omega_c = 2\pi \times 4\,\mathrm{MHz}$ (blue solid line) and $\Omega_c = 2\pi \times 8\,\mathrm{MHz}$ (red dotted line), with $N_a = 1.1 \times 10^{9}\,\mathrm{cm}^{-3}$ (dot M), $N_a = 3.1 \times 10^{8}\,\mathrm{cm}^{-3}$ (dot N), $\Omega_p = 0.2\Gamma_{13}$, and $\Omega_a = 10\,\mathrm{MHz}$. Other parameters are the same as in Fig. 2.

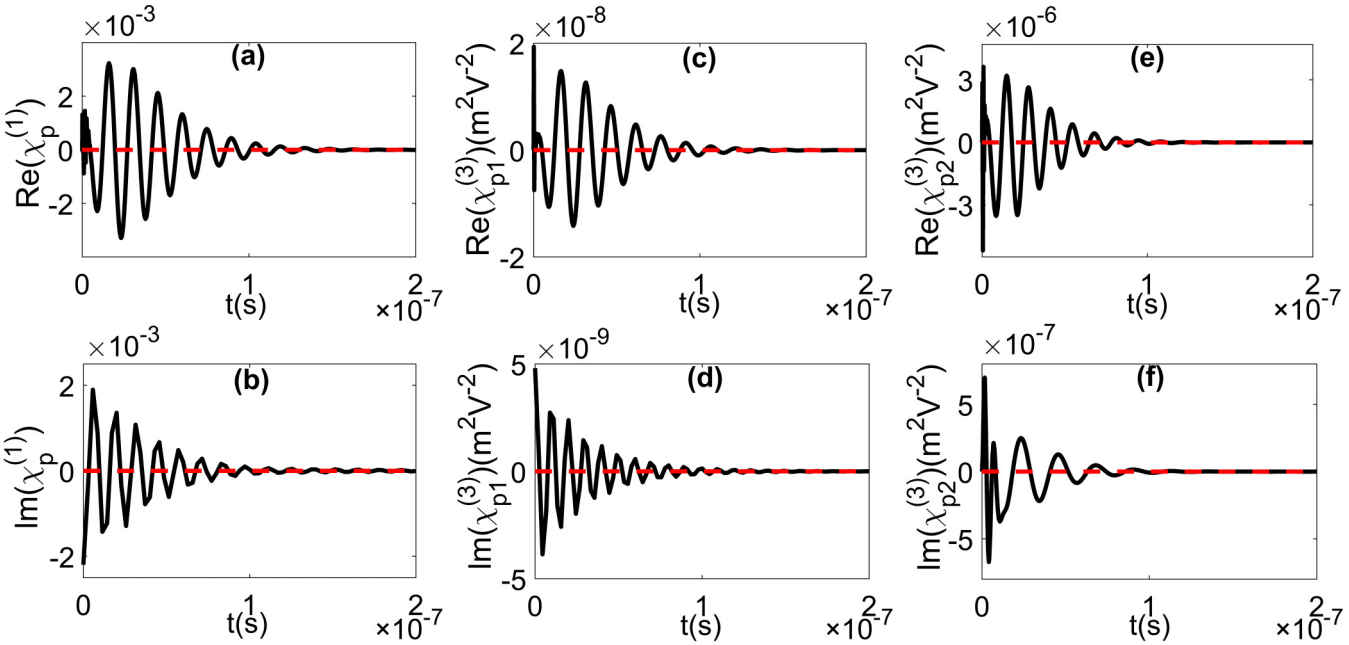

FIG. 5. Time evolution of the linear susceptibility $\chi_p^{(1)}$ and the third-order nonlinear susceptibility of the probe field $\chi_{p1}^{(3)}$ and $\chi_{p2}^{(3)}$. Parameters are $\Omega_p = 0.05 \times \Gamma_{13}\,\mathrm{s}^{-1}$, $\Omega_c = 16\pi \times 10^6\,\mathrm{s}^{-1}$, $\Omega_a = 250\,\mathrm{MHz}$, $\Gamma_{21} = 0.2\pi \times 10^6\,\mathrm{s}^{-1}$, $\Gamma_3 = \Gamma_{13} + \Gamma_{23} = 40\pi \times 10^6\,\mathrm{s}^{-1}$, $\Gamma_4 = \Gamma_{34} = 10\pi \times 10^6\,\mathrm{s}^{-1}$, $N_a = 1.0 \times 10^{12}\,\mathrm{cm}^{-3}$, and $K = 3.02 \times 10^5\,\mathrm{s}^{-1}$. (a,b) The real part and the imaginary part of the linear susceptibility $\chi_p^{(1)}$, respectively. (c,d) The real part and the imaginary part of the self-Kerr nonlinear susceptibility of the probe field $\chi_{p1}^{(3)}$, respectively. (e,f) The real part and the imaginary part of the self-Kerr nonlinear susceptibility of the probe field $\chi_{p2}^{(3)}$, respectively. Red dashed line is the steady-state value of the susceptibility response function.

the effect of the "soft core," resulting from a strong Rydberg blockade effect, where the excitation to Rydberg states is completely blockaded for very closed atoms. On the other hand, when $N_a = 3.1 \times 10^8\,\mathrm{cm}^{-3}$ (dot N, $r_{AB} = 8.2\,\mu\mathrm{m}$), the Rydberg interaction is completely absent; we get the longest response time $T_R = 1.45\,\mu\mathrm{s}$, which is a critical point for the existence of Rydberg interactions. Additionally, from Fig. 4(c) we know that the response time T_R increases with the control field.

Figure 5 shows the evolution of the linear susceptibility $\chi_p^{(1)}$ and the third-order nonlinear susceptibility of the probe field $\chi_{p1}^{(3)}$ and $\chi_{p2}^{(3)}$. Parameters are Ω_p=$0.05\times\Gamma_{13}\,\mathrm{s}^{-1}$, $\Omega_c = 16\pi \times 10^6\,\mathrm{s}^{-1}$, $\Omega_a = 250\,\mathrm{MHz}$, $\Gamma_{21} = 0.2\pi \times 10^6\,\mathrm{s}^{-1}$, $\Gamma_3 = \Gamma_{13} + \Gamma_{23} = 40\pi \times 10^6\,\mathrm{s}^{-1}$, Γ_4=$\Gamma_{34} = 10\pi \times 10^6\,\mathrm{s}^{-1}$, $N_a = 1.0 \times 10^{12}\,\mathrm{cm}^{-3}$, and $K = 3.02 \times 10^5\,\mathrm{s}^{-1}$. Figures 5(a) and 5(b) show the linear transient behavior of the real part and the imaginary part of susceptibility $\chi_p^{(1)}$. One can see that $\chi_p^{(1)}$ oscillates in the initial time interval of the order of 10^{-7} s and decays to nearly zero rapidly, as time progresses. Figures 5(c) and 5(d) show the result of the transient behavior of the self-Kerr nonlinear susceptibility of the probe field $\chi_{p1}^{(3)}$. Similarly, one can see that $\chi_{p1}^{(3)}$ oscillates in the initial time interval of the order of 10^{-7} s and decays to nearly zero ($\chi_p^{(3)} = 2.46 \times 10^{-8}\,\mathrm{m}^2\,\mathrm{V}^{-2}$) rapidly as time increases; this happens faster than in the conventional EIT with $\Delta_2 = \Delta_3 = \Delta_4 = 0$ [42]. The physical reason of nearly vanishing $\chi_p^{(3)}$ after the transient evolution is due to the EIT-induced quantum interference effect, which greatly suppresses the absorption of the probe field. In Figs. 5(e) and 5(f), one can see that the nonlinear third-order optical susceptibility $\chi_{p2}^{(3)}$ performs an oscillation in the initial time interval of the order of 10^{-7} s and decays nearly to zero rapidly, as time increases. However, the nonlocal optical nonlinearity susceptibility ($\chi_{p2}^{(3)} = 2.46 \times 10^{-8}\,\mathrm{m}^2\,\mathrm{V}^{-2}$) with the Rydberg interaction is faster than the local optical nonlinearity susceptibility ($\chi_{p1}^{(3)} = 1.7 \times 10^{-11}\,\mathrm{m}^2\,\mathrm{V}^{-2}$) [see Figs. 5(c) and 5(e)].

Figure 6 shows the nonlinear transient behavior of the fifth-order nonlinear susceptibility of the probe field $\chi_{p1}^{(5)}$ and $\chi_{p2}^{(5)}$. The system parameters are the same as in Fig. 5. From Figures 6(a) and 6(b), one can see that the nonlinear fifth-order optical susceptibility $\chi_{p1}^{(5)}$ performs an oscillation in the initial time interval of the order of 10^{-6} s and decays nearly to zero rapidly, as time increases. Similarly, one can see that for the fifth-order optical susceptibility $\chi_{p2}^{(5)}$, the nonlocal optical nonlinearity with the Rydberg interaction possesses a faster response than the local optical nonlinearity $\chi_{p1}^{(5)}$ [see Fig. 6]. Furthermore, it is shown that the nonlinear response time of the fifth-order optical susceptibility $\chi_p^{(5)}$ is longer than that of the third-order optical susceptibility $\chi_p^{(3)}$.

In order to obtain more information about the character of the Rydberg EIT, we calculate the stable values of the third-order and the fifth-order nonlinear optical susceptibilities in Table II; the system parameters are the same as in Figs. 5 and 6. From Table II, one can see that for the given high atomic density (i.e., $N_a = 1.0 \times 10^{12}\,\mathrm{cm}^{-3}$), the nonlinear optical susceptibilities with interaction (i.e., $\chi_{p2}^{(3)}$ and $\chi_{p2}^{(5)}$) are three

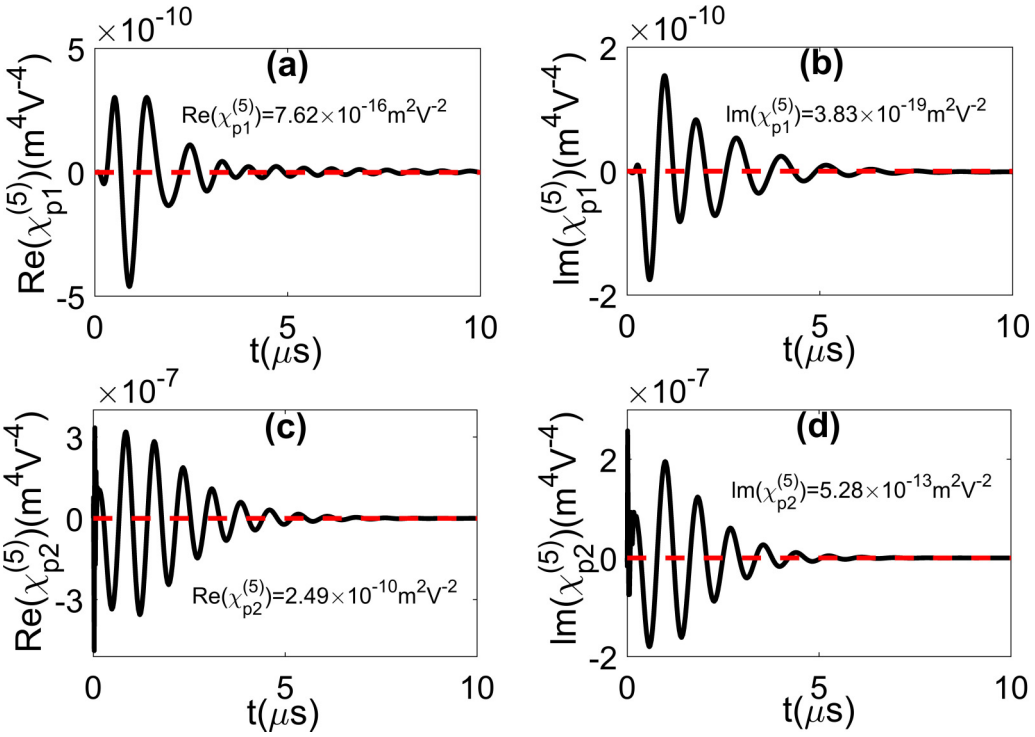

FIG. 6. Time evolution of the fifth-order nonlinear susceptibilities of the probe field $\chi_{p1}^{(5)}$ and $\chi_{p2}^{(5)}$. (a,b) The real part and the imaginary part of the fifth-order nonlinear susceptibility of the probe field $\chi_{p1}^{(5)}$, respectively. (c,d) The real part and the imaginary part of the fifth-order nonlinear susceptibility of the probe field $\chi_{p2}^{(5)}$, respectively. The system parameters are the same as in Fig. 5.

and six orders of magnitude greater than those contributed by the photon-atom interaction (i.e., $\chi_{p1}^{(3)}$ and $\chi_{p1}^{(5)}$), respectively. Thus, at this atomic density the Rydberg-Rydberg interaction plays a leading role in the contribution of the nonlinear optical susceptibilities in the system [see Table II, and Figs. 5(c)–5(f) and 6]. In particular, the fifth-order nonlinear optical susceptibility originating from the Rydberg-Rydberg interaction can reach the order of magnitude of 10^{-10} m^4 V^{-4}. Furthermore, it is shown that the imaginary parts of the all nonlinear optical susceptibilities are much smaller than their corresponding real parts, which means that the nonlinear absorption can be suppressed in the nonlinear optical processes of the system. The physical reason for this suppression of the nonlinear absorption is the quantum interference effect induced by the control field. For a low atomic density ($N_a = 1.0 \times 10^8$ cm^{-3}), Rydberg interaction can be close to zero. From Eq. (4), one can see that $\chi_{p1}^{(3)}$ and $\chi_{p1}^{(5)}$ have a linear dependence on the atomic density N_a, which is only 10^{-4} times the high atom density.

IV. CONCLUSION

In conclusion, we have studied the transient linear and nonlinear optical response properties of the EIT in a cold Rydberg atomic gas. We have demonstrated that the transient behavior (especially, the third- and fifth-order susceptibilities of the probefield) and the steady-state EIT spectrum of the system depend strongly on the Rydberg interaction. In particular, the response speed of the Rydberg EIT can be increased by increasing the probe-field intensity and decreased by increasing the control-field intensity. Further, the response speed of the Rydberg-EIT may be six times faster than the conventional EIT without Rydberg interaction, and the nonlinear response time of the fifth-order optical susceptibility is longer than that of the third-order optical susceptibility. The results reveal that the Rydberg blockade effect plays a significant role in increasing the response speed of the Rydberg EIT. The fast-responding Rydberg EIT by using the strong, tunable Rydberg interaction found here is useful not only for a deeper understanding of the nonequilibrium many-body dynamics of

TABLE II. Real part Re($\chi_{p\alpha}^{(j)}$) and imaginary part Im($\chi_{p\alpha}^{(j)}$) ($j = 3, 5; \alpha = 1, 2$) of the third-order and the fifth-order optical susceptibilities of the Rydberg-EIT system obtained for the realistic system parameters given in the text.

	Real part	Imaginary part	Contributed by
$\chi_{p1}^{(3)}$	-1.7×10^{-11} m^2 V^{-2}	-3.5×10^{-13} m^2 V^{-2}	Photon-atom interaction
$\chi_{p2}^{(3)}$	2.46×10^{-8} m^2 V^{-2}	5.21×10^{-10} m^2 V^{-2}	Rydberg-Rydberg interaction
$\chi_{p1}^{(5)}$	7.62×10^{-16} m^4 V^{-4}	3.83×10^{-19} m^4 V^{-4}	Photon-atom interaction
$\chi_{p2}^{(5)}$	2.49×10^{-10} m^4 V^{-4}	5.28×10^{-13} m^{4}V^{-4}	Rydberg-Rydberg interaction

Rydberg atoms, but also for practical applications in quantum information processing based on the cold Rydberg atoms.

ACKNOWLEDGMENTS

This work is supported in China by the National Natural Science Foundation under Grant No. 11847103, the Research Foundation of Engineering Master Degree of Hubei University of Science and Technology (Grant No. 2018-19GZ02), and Scientific Research and Innovation team of Hubei University of Science and Technology (Grant No. 180024). Work in Qatar is supported by Project No. NPRP 11S-1126-170033 with the Qatar National Research Fund (a member of the Qatar Foundation).

Y.-W.G. and S.-L.X. contributed equally to this work.

APPENDIX A: EQUATIONS OF MOTION FOR TWO-BODY CORRELATORS

The explicit form of equations of motion for two-body correlators density matrix elements reads as follows:

$$\left(i\frac{\partial}{\partial t}+2d_{21}\right)\rho_{21,21}+2\Omega_c^*\rho_{31,21}-2\Omega_p\rho_{23,21}=0, \tag{A1}$$

$$\left(i\frac{\partial}{\partial t}+d_{21}+d_{31}\right)\rho_{21,31}+\Omega_p\left(\rho_{21}-\rho_{21,22}-2\rho_{21,33}-\rho_{23,31}-\rho_{21,44}\right)+\Omega_c\rho_{21,21}+\Omega_c^*\rho_{31,31}+\Omega_a^*\rho_{21,41}=0, \tag{A2}$$

$$\left(i\frac{\partial}{\partial t}+d_{21}+d_{41}\right)\rho_{21,41}-\Omega_p\left(\rho_{23,41}+\rho_{21,43}\right)+\Omega_c^*\rho_{31,41}+\Omega_a\rho_{21,31}=0, \tag{A3}$$

$$\left(i\frac{\partial}{\partial t}+2d_{31}\right)\rho_{31,31}+2\Omega_p(\rho_{31}-\rho_{31,22}-2\rho_{31,33}-\rho_{31,44})+2\Omega_c\rho_{21,31}+2\Omega_a^*\rho_{41,31}=0, \tag{A4}$$

$$\left(i\frac{\partial}{\partial t}+d_{31}+d_{41}\right)\rho_{31,41}+\Omega_p(\rho_{41}-\rho_{22,41}-2\rho_{33,41}-\rho_{44,41}-\rho_{31,43})+\Omega_c\rho_{21,41}+\Omega_a^*\rho_{41,41}+\Omega_a\rho_{31,31}=0, \tag{A5}$$

$$\left(i\frac{\partial}{\partial t}+2d_{41}\right)\rho_{41,41}+2\Omega_a\rho_{31,41}-2\Omega_p\rho_{43,41}-V\rho_{41,41}=0, \tag{A6}$$

$$\left(i\frac{\partial}{\partial t}+d_{21}+d_{12}\right)\rho_{21,12}+\Omega_p^*\rho_{21,32}-\Omega_p\rho_{23,12}+\Omega_c^*\rho_{31,12}-\Omega_c\rho_{21,13}=0, \tag{A7}$$

$$\left(i\frac{\partial}{\partial t}+d_{21}+d_{13}\right)\rho_{21,13}-\Omega_p\rho_{23,13}+\Omega_p^*(-\rho_{21}+2\rho_{21,33}+\rho_{21,22}+\rho_{21,44})+\Omega_c^*(\rho_{31,13}-\rho_{21,12})-\Omega_a\rho_{21,14}=0, \tag{A8}$$

$$\left(i\frac{\partial}{\partial t}+d_{21}+d_{14}\right)\rho_{21,14}+\Omega_p^*\rho_{21,34}-\Omega_p\rho_{23,14}+\Omega_c^*\rho_{31,14}-\Omega_a^*\rho_{21,13}=0, \tag{A9}$$

$$\left(i\frac{\partial}{\partial t}+d_{31}+d_{12}\right)\rho_{31,12}+\Omega_p(\rho_{12}-2\rho_{33,12}-\rho_{22,12}-\rho_{44,12})+\Omega_c(\rho_{21,12}-\rho_{31,13})+\Omega_p^*\rho_{31,32}+\Omega_a^*\rho_{41,12}=0, \tag{A10}$$

$$\left(i\frac{\partial}{\partial t}+d_{31}+d_{13}\right)\rho_{31,13}+\Omega_p(\rho_{13}-2\rho_{33,13}-\rho_{22,13}-\rho_{44,13})+\Omega_p^*(-\rho_{31}+2\rho_{31,33}+\rho_{31,22}+\rho_{31,44})$$
$$+\Omega_c\rho_{21,13}-\Omega_c^*\rho_{31,12}+\Omega_a^*\rho_{41,13}-\Omega_a\rho_{31,14}=0, \tag{A11}$$

$$\left(i\frac{\partial}{\partial t}+d_{31}+d_{14}\right)\rho_{31,14}+\Omega_p(\rho_{14}-\rho_{22,14}-2\rho_{33,14}-\rho_{44,14})+\Omega_p^*\rho_{31,34}+\Omega_c\rho_{21,14}+\Omega_a^*(\rho_{41,14}-\rho_{31,13})=0, \tag{A12}$$

$$\left(i\frac{\partial}{\partial t}+d_{41}+d_{12}\right)\rho_{41,12}-\Omega_p\rho_{43,13}+\Omega_p^*\rho_{41,32}-\Omega_c\rho_{41,13}+\Omega_a\rho_{31,12}=0, \tag{A13}$$

$$\left(i\frac{\partial}{\partial t}+d_{41}+d_{13}\right)\rho_{41,13}-\Omega_p\rho_{43,13}+\Omega_p^*(-\rho_{41}+2\rho_{41,33}+\rho_{41,22}+\rho_{41,44})-\Omega_c^*\rho_{41,12}+\Omega_a(\rho_{31,13}-\rho_{41,14})=0, \tag{A14}$$

$$\left(i\frac{\partial}{\partial t}+d_{41}+d_{14}\right)\rho_{41,14}-\Omega_p\rho_{43,14}+\Omega_p^*\rho_{41,34}+\Omega_a\rho_{31,14}-\Omega_a^*\rho_{41,13}=0, \tag{A15}$$

$$\left(i\frac{\partial}{\partial t}+d_{21}\right)\rho_{22,21}-i\Gamma_{21}(\rho_{21}-\rho_{22,21}-\rho_{33,21}-\rho_{44,21})-i\Gamma_{23}\rho_{33,21}-\Omega_p\rho_{22,23}+\Omega_c^*(\rho_{32,21}+\rho_{22,31})-\Omega_c\rho_{23,21}=0, \tag{A16}$$

$$\left(i\frac{\partial}{\partial t}+d_{31}\right)\rho_{22,31}-i\Gamma_{21}(\rho_{31}-\rho_{22,31}-\rho_{33,31}-\rho_{44,31})-i\Gamma_{23}\rho_{33,31}+\Omega_p(\rho_{22}-\rho_{22,22}-\rho_{22,44}-2\rho_{22,33})$$
$$+\Omega_c(\rho_{22,21}-\rho_{23,31})+\Omega_c^*\rho_{32,31}+\Omega_a^*\rho_{22,41}=0, \tag{A17}$$

$$\left(i\frac{\partial}{\partial t}+d_{41}\right)\rho_{22,41}-i\Gamma_{21}(\rho_{41}-\rho_{22,41}-\rho_{33,41}-\rho_{44,41})-i\Gamma_{23}\rho_{33,41}-\Omega_p\rho_{22,43}+\Omega_c^*\rho_{32,41}-\Omega_c\rho_{23,41}+\Omega_a\rho_{22,31}=0, \tag{A18}$$

$$\left(i\frac{\partial}{\partial t}+d_{23}+d_{21}\right)\rho_{23,21}-\Omega_p\rho_{23,23}-\Omega_p^*\rho_{21,21}+\Omega_c^*(\rho_{33,21}+\rho_{23,31}-\rho_{22,21})-\Omega_a\rho_{24,21}=0, \tag{A19}$$

$$\left(i\frac{\partial}{\partial t}+d_{23}+d_{31}\right)\rho_{23,31}+\Omega_p(\rho_{23}-\rho_{23,22}-\rho_{23,44}-2\rho_{23,33})-\Omega_p^*\rho_{21,31}+\Omega_c^*(\rho_{33,31}-\rho_{22,31})+\Omega_c\rho_{23,21}+\Omega_a^*\rho_{23,41}-\Omega_a\rho_{24,31}=0, \tag{A20}$$

$$\left(i\frac{\partial}{\partial t}+d_{23}+d_{41}\right)\rho_{23,41}-\Omega_p\rho_{23,43}-\Omega_p^*\rho_{21,41}+\Omega_c^*(\rho_{33,41}-\rho_{22,41})+\Omega_c(\rho_{23,31}-\rho_{24,41})=0, \tag{A21}$$

$$\left(i\frac{\partial}{\partial t}+d_{24}+d_{21}\right)\rho_{24,21}-\Omega_p\rho_{24,23}+\Omega_c^*(\rho_{34,21}+\rho_{24,31})-\Omega_a^*\rho_{23,21}=0, \tag{A22}$$

$$\left(i\frac{\partial}{\partial t}+d_{24}+d_{31}\right)\rho_{24,31}+\Omega_p(\rho_{24}-\rho_{24,44}-\rho_{24,22}-2\rho_{24,33})+\Omega_c\rho_{24,21}+\Omega_c^*\rho_{34,31}+\Omega_a^*(\rho_{24,41}-\rho_{23,31})=0, \tag{A23}$$

$$\left(i\frac{\partial}{\partial t}+d_{24}+d_{41}\right)\rho_{24,41}-\Omega_p\rho_{24,43}+\Omega_c^*\rho_{34,41}+\Omega_a\rho_{24,31}-\Omega_a^*\rho_{23,41}=0, \tag{A24}$$

$$\left(i\frac{\partial}{\partial t}+d_{32}+d_{21}\right)\rho_{32,21}+\Omega_p(\rho_{12,21}-\rho_{32,23})+\Omega_c(\rho_{22,21}-\rho_{33,21})+\Omega_c^*\rho_{32,31}+\Omega_a^*\rho_{42,21}=0, \tag{A25}$$

$$\left(i\frac{\partial}{\partial t}+d_{32}+d_{31}\right)\rho_{32,31}+\Omega_p(\rho_{12,31}+\rho_{32}-2\rho_{32,33}-\rho_{32,22}-\rho_{32,44})+\Omega_c(\rho_{23,31}+\rho_{32,21}-\rho_{33,31})+\Omega_a^*(\rho_{42,31}+\rho_{32,41})=0, \tag{A26}$$

$$\left(i\frac{\partial}{\partial t}+d_{32}+d_{41}\right)\rho_{32,41}+\Omega_p(\rho_{12,41}-\rho_{32,43})+\Omega_c(\rho_{22,41}-\rho_{33,41})+\Omega_a\rho_{32,31}+\Omega_a^*\rho_{42,41}=0, \tag{A27}$$

$$\left(i\frac{\partial}{\partial t}+i\Gamma_{13}+i\Gamma_{23}+d_{21}\right)\rho_{33,21}-i\Gamma_{34}\rho_{44,21}+\Omega_p(\rho_{13,21}-\rho_{33,23})-\Omega_p^*\rho_{31,21}+\Omega_c\rho_{23,21}+\Omega_c^*(\rho_{33,31}-\rho_{32,21})+\Omega_a^*\rho_{43,21}-\Omega_a\rho_{34,21}=0, \tag{A28}$$

$$\left(i\frac{\partial}{\partial t}+i\Gamma_{13}+i\Gamma_{23}+d_{31}\right)\rho_{33,31}-i\Gamma_{34}\rho_{44,31}+\Omega_p(\rho_{13,31}+\rho_{33}-2\rho_{33,33}-\rho_{33,22}-\rho_{33,44})-\Omega_p^*\rho_{31,31}+\Omega_c(\rho_{23,31}+\rho_{33,21})-\Omega_c^*\rho_{32,31}+\Omega_a^*(\rho_{43,31}+\rho_{33,41})-\Omega_a\rho_{34,31}=0, \tag{A29}$$

$$\left(i\frac{\partial}{\partial t}+i\Gamma_{13}+i\Gamma_{23}+d_{41}\right)\rho_{33,41}-i\Gamma_{34}\rho_{44,41}+\Omega_p(\rho_{13,41}-\rho_{33,43})-\Omega_p^*\rho_{31,41}+\Omega_c\rho_{23,41}-\Omega_c^*\rho_{32,41}+\Omega_a(\rho_{33,31}-\rho_{34,41})+\Omega_a^*\rho_{43,41}=0, \tag{A30}$$

$$\left(i\frac{\partial}{\partial t}+d_{34}+d_{21}\right)\rho_{34,21}+\Omega_p(\rho_{14,21}-\rho_{34,23})+\Omega_c\rho_{24,21}+\Omega_c^*\rho_{34,31}+\Omega_a^*(\rho_{44,21}-\rho_{33,21})=0, \tag{A31}$$

$$\left(i\frac{\partial}{\partial t}+d_{34}+d_{31}\right)\rho_{34,31}+\Omega_p(\rho_{14,31}+\rho_{34}-2\rho_{34,33}-\rho_{34,22}-\rho_{34,44})+\Omega_c(\rho_{24,31}+\rho_{34,21})+\Omega_a^*(\rho_{44,31}+\rho_{34,41}-\rho_{33,31})=0, \tag{A32}$$

$$\left(i\frac{\partial}{\partial t}+d_{34}+d_{41}\right)\rho_{34,41}+\Omega_p(\rho_{14,41}-\rho_{34,43})+\Omega_c\rho_{24,41}+\Omega_a^*(\rho_{44,41}-\rho_{33,41})+\Omega_a\rho_{34,31}=0, \tag{A33}$$

$$\left(i\frac{\partial}{\partial t}+d_{42}+d_{21}\right)\rho_{42,21}-\Omega_p\rho_{42,23}-\Omega_c\rho_{43,21}+\Omega_c^*\rho_{42,31}+\Omega_a\rho_{32,21}=0, \tag{A34}$$

$$\left(i\frac{\partial}{\partial t}+d_{42}+d_{31}\right)\rho_{42,31}+\Omega_p(\rho_{42}-2\rho_{42,33}-\rho_{42,22}-\rho_{42,44})+\Omega_c(\rho_{42,21}-\rho_{43,31})+\Omega_a^*\rho_{42,41}+\Omega_a\rho_{32,31}=0, \tag{A35}$$

$$\left(i\frac{\partial}{\partial t}+d_{42}+d_{41}-V\right)\rho_{42,41}-\Omega_p\rho_{42,43}-\Omega_c\rho_{43,41}+\Omega_a(\rho_{32,41}+\rho_{42,31})=0, \tag{A36}$$

$$\left(i\frac{\partial}{\partial t}+d_{43}+d_{21}\right)\rho_{43,21}-\Omega_p\rho_{43,23}-\Omega_p^*\rho_{41,21}+\Omega_c^*(\rho_{43,31}-\rho_{42,21})+\Omega_a(\rho_{33,21}-\rho_{44,21})=0, \tag{A37}$$

$$\left(i\frac{\partial}{\partial t}+d_{43}+d_{31}\right)\rho_{43,31}+\Omega_p(\rho_{43}-2\rho_{43,33}-\rho_{43,22}-\rho_{43,44})-\Omega_p^*\rho_{41,31}+\Omega_c\rho_{43,21}-\Omega_c^*\rho_{42,31}+\Omega_a^*\rho_{43,41}$$
$$+\Omega_a(\rho_{33,31}-\rho_{44,31})=0, \tag{A38}$$

$$\left(i\frac{\partial}{\partial t}+d_{43}+d_{41}-V\right)\rho_{43,41}-\Omega_p\rho_{43,43}-\Omega_p^*\rho_{41,41}-\Omega_c^*\rho_{42,41}+\Omega_a(\rho_{33,41}+\rho_{43,31}-\rho_{44,41})=0, \tag{A39}$$

$$\left(i\frac{\partial}{\partial t}+i\Gamma_{34}+d_{21}\right)\rho_{44,21}-\Omega_p\rho_{44,23}+\Omega_c^*\rho_{44,31}+\Omega_a\rho_{34,21}-\Omega_a^*\rho_{43,21}=0, \tag{A40}$$

$$\left(i\frac{\partial}{\partial t}+i\Gamma_{34}+d_{31}\right)\rho_{44,31}+\Omega_p(\rho_{44}-2\rho_{44,33}-\rho_{22,44}-\rho_{44,44})+\Omega_c\rho_{44,21}+\Omega_a^*(\rho_{44,41}-\rho_{43,31})+\Omega_a\rho_{34,31}=0, \tag{A41}$$

$$\left(i\frac{\partial}{\partial t}+i\Gamma_{34}+d_{41}-V\right)\rho_{44,41}-\Omega_p\rho_{44,43}+\Omega_a(\rho_{44,31}+\rho_{34,41})-\Omega_a^*\rho_{43,41}=0, \tag{A42}$$

APPENDIX B: MANY-ATOM MODEL AND REDUCED DENSITY MATRIX APPROACH

Steps for solving the equations of motion for the one- and two-body correlators in the many-atom model are the following.

First-order approximation: At this order, we need to obtain the one-body correlators $\rho_{j1}^{(1)}=a_{j1}^{(1)}{\Omega_p}^{(1)}$ $(\alpha=2,3,4)$ only, which satisfy

$$-i\frac{\partial}{\partial t_0}\begin{bmatrix}a_{21}^{(1)}\\a_{31}^{(1)}\\a_{41}^{(1)}\end{bmatrix}=\begin{bmatrix}d_{21}&\Omega_c^*&0\\\Omega_c&d_{31}&\Omega_a^*\\0&\Omega_a&d_{41}\end{bmatrix}\begin{bmatrix}a_{21}^{(1)}\\a_{31}^{(1)}\\a_{41}^{(1)}\end{bmatrix}+\begin{bmatrix}0\\1\\0\end{bmatrix}, \tag{B1}$$

with the initial condition $a_{21}^{(1)}(0)=0$, $a_{31}^{(1)}(0)=-1/d_{31}$, $a_{41}^{(1)}(0)=0$. Here $t_0=t$ is the fast time variable.

Second-order approximation: We will find the lowest-order solution of the two-body correlators that start at this order. The first set of equations governing the two-body correlators $\rho_{j1,l1}^{(2)}=a_{j1,l1}^{(2)}|{\Omega_p}^{(1)}|^2$ $(j,l=2,3,4)$ is given by

$$-i\frac{\partial}{\partial t_0}\begin{bmatrix}a_{21,21}^{(2)}\\a_{21,31}^{(2)}\\a_{21,41}^{(2)}\\a_{31,31}^{(2)}\\a_{31,41}^{(2)}\\a_{41,41}^{(2)}\end{bmatrix}=\begin{bmatrix}2d_{21}&2\Omega_c^*&0&0&0&0\\\Omega_c&d_{21}+d_{31}&\Omega_a^*&\Omega_c^*&0&0\\0&\Omega_a&d_{21}+d_{41}&0&\Omega_c^*&0\\0&2\Omega_c&0&2d_{31}&2\Omega_a^*&0\\0&0&\Omega_c&\Omega_a&d_{31}+d_{41}&\Omega_a^*\\0&0&0&0&2\Omega_a&2d_{41}-V\end{bmatrix}\begin{bmatrix}a_{21,21}^{(2)}\\a_{21,31}^{(2)}\\a_{21,41}^{(2)}\\a_{31,31}^{(2)}\\a_{31,41}^{(2)}\\a_{41,41}^{(2)}\end{bmatrix}+\begin{bmatrix}0\\a_{21}^{(1)}\\0\\2a_{31}^{(1)}\\a_{41}^{(1)}\\0\end{bmatrix}, \tag{B2}$$

with the initial conditions $a_{31,31}^{(2)}(0)=1/{d_{31}}^2$, and other $a_{j1,l1}^{(2)}(0)=0$. The second set of equations governing the two-body correlators $\rho_{j1,1l}^{(2)}=a_{j1,1l}^{(2)}|{\Omega_p}^{(1)}|^2$ $(j,l=2,3,4)$ reads as

$$-i\frac{\partial}{\partial t_0}\begin{bmatrix}a_{21,12}^{(2)}\\a_{21,13}^{(2)}\\a_{21,14}^{(2)}\\a_{31,12}^{(2)}\\a_{31,13}^{(2)}\\a_{31,14}^{(2)}\\a_{41,12}^{(2)}\\a_{41,13}^{(2)}\\a_{41,14}^{(2)}\end{bmatrix}=\begin{bmatrix}M_{11}&-\Omega_c&0&\Omega_c^*&0&0&0&0&0\\-\Omega_c^*&M_{12}&-\Omega_a&0&\Omega_c^*&0&0&0&0\\0&-\Omega_a^*&M_{13}&0&0&\Omega_c^*&0&0&0\\\Omega_c&0&0&M_{14}&-\Omega_c&0&\Omega_a^*&0&0\\0&\Omega_c&0&-\Omega_c^*&M_{15}&-\Omega_a&0&\Omega_a^*&0\\0&0&\Omega_c&0&-\Omega_a^*&M_{16}&0&0&\Omega_a^*\\0&0&0&\Omega_a&0&0&M_{17}&-\Omega_c&0\\0&0&0&0&\Omega_a&0&-\Omega_c^*&M_{18}&-\Omega_a\\0&0&0&0&0&\Omega_a&0&-\Omega_a^*&M_{19}\end{bmatrix}\begin{bmatrix}a_{21,12}^{(2)}\\a_{21,13}^{(2)}\\a_{21,14}^{(2)}\\a_{31,12}^{(2)}\\a_{31,13}^{(2)}\\a_{31,14}^{(2)}\\a_{41,12}^{(2)}\\a_{41,13}^{(2)}\\a_{41,14}^{(2)}\end{bmatrix}+\begin{bmatrix}0\\-a_{21}^{(1)}\\0\\a_{21}^{(1)*}\\a_{31}^{(1)*}-a_{31}^{(1)}\\a_{41}^{(1)*}\\0\\-a_{41}^{(1)}\\0\end{bmatrix}, \tag{B3}$$

where $M_{11}=d_{21}+d_{12}$, $M_{12}=d_{21}+d_{13}$, $M_{13}=d_{21}+d_{14}$, $M_{14}=d_{31}+d_{12}$, $M_{15}=d_{31}+d_{13}$, $M_{16}=d_{31}+d_{14}$, $M_{17}=d_{41}+d_{12}$, $M_{18}=d_{41}+d_{13}$, and $M_{19}=d_{41}+d_{14}$, and the initial conditions are $a_{31,13}^{(2)}(0)=|\Omega_p^{(1)}/d_{31}|^2$, and other $a_{j1,1l}^{(2)}(0)=0$. The

equation of the one-body correlators $\rho_{jl}^{(2)}=a_{jl}^{(2)}|\Omega_p{}^{(1)}|^2$ $(j,l=2,3,4)$ at this order is

$$-i\frac{\partial}{\partial t_0}\begin{bmatrix} a_{22}^{(2)} \\ a_{33}^{(2)} \\ a_{44}^{(2)} \\ a_{23}^{(2)} \\ a_{24}^{(2)} \\ a_{32}^{(2)} \\ a_{34}^{(2)} \\ a_{42}^{(2)} \\ a_{43}^{(2)} \end{bmatrix} = \begin{bmatrix} 0 & -i\Gamma_{23} & 0 & -\Omega_c & 0 & \Omega_c^* & 0 & 0 & 0 \\ 0 & i\Gamma_3 & -i\Gamma_{34} & \Omega_c & 0 & -\Omega_c^* & -\Omega_a & 0 & \Omega_a^* \\ 0 & 0 & i\Gamma_{34} & 0 & 0 & 0 & \Omega_a & 0 & -\Omega_a^* \\ -\Omega_c^* & \Omega_c^* & 0 & d_{23} & -\Omega_a & 0 & 0 & 0 & 0 \\ 0 & 0 & 0 & -\Omega_a^* & d_{24} & 0 & \Omega_c^* & 0 & 0 \\ \Omega_c & -\Omega_c & 0 & 0 & 0 & d_{32} & 0 & \Omega_a^* & 0 \\ 0 & -\Omega_a^* & \Omega_a^* & 0 & \Omega_c & 0 & d_{34} & 0 & 0 \\ 0 & 0 & 0 & 0 & 0 & \Omega_a & 0 & d_{42} & -\Omega_c \\ 0 & \Omega_a & -\Omega_a & 0 & 0 & 0 & 0 & -\Omega_c^* & d_{43} \end{bmatrix} \begin{bmatrix} a_{22}^{(2)} \\ a_{33}^{(2)} \\ a_{44}^{(2)} \\ a_{23}^{(2)} \\ a_{24}^{(2)} \\ a_{32}^{(2)} \\ a_{34}^{(2)} \\ a_{42}^{(2)} \\ a_{43}^{(2)} \end{bmatrix} + \begin{bmatrix} i\Gamma_{21}(a_{22}^{(2)}+a_{33}^{(2)}+a_{44}^{(2)}) \\ a_{31}^{(1)*}-a_{31}^{(1)} \\ 0 \\ -a_{21}^{(1)} \\ 0 \\ a_{21}^{(1)*} \\ a_{41}^{(1)*} \\ 0 \\ -a_{41}^{(1)} \end{bmatrix}, \tag{B4}$$

with the initial conditions $a_{33}^{(2)}(0)=2\gamma_{31}|\Omega_p^{(1)}|^2/(\Gamma_{13}|d_{31}|^2)$ and other $a_{jl}^{(2)}(0)=0$. The solution of $\rho_{11}^{(2)}$ is given by $\rho_{11}^{(2)}=-\rho_{22}^{(2)}-\rho_{33}^{(2)}-\rho_{44}^{(2)}$.

Third-order approximation: At this order, equations governing the two-body correlators $\rho_{jl,\mu 1}^{(3)}=a_{jl,\mu 1}^{(3)}|\Omega_p{}^{(1)}|^2\Omega_p{}^{(1)}$ $(j,l,\mu=2,3,4)$ are given by

$$-i\frac{\partial}{\partial t_0}\begin{bmatrix} a_{22,21}^{(3)} \\ a_{22,31}^{(3)} \\ a_{22,41}^{(3)} \\ a_{23,21}^{(3)} \\ a_{23,31}^{(3)} \\ a_{23,41}^{(3)} \\ \vdots \\ a_{43,21}^{(3)} \\ a_{43,31}^{(3)} \\ a_{43,41}^{(3)} \\ a_{44,21}^{(3)} \\ a_{44,31}^{(3)} \\ a_{44,41}^{(3)} \end{bmatrix} = \begin{pmatrix} M_{21} & \Omega_c^* & 0 & -\Omega_c & 0 & 0 & & 0 & 0 & 0 & i\Gamma_{21} & 0 & 0 \\ \Omega_c & M_{22} & \Omega_a^* & 0 & -\Omega_c & 0 & & 0 & 0 & 0 & 0 & i\Gamma_{21} & 0 \\ 0 & \Omega_a & M_{23} & 0 & 0 & -\Omega_c & & 0 & 0 & 0 & 0 & 0 & i\Gamma_{21} \\ -\Omega_c^* & 0 & 0 & M_{24} & \Omega_c^* & 0 & \cdots & 0 & 0 & 0 & 0 & 0 & 0 \\ 0 & -\Omega_c^* & 0 & \Omega_c^* & M_{25} & \Omega_a^* & & 0 & 0 & 0 & 0 & 0 & 0 \\ 0 & 0 & -\Omega_c^* & 0 & \Omega_a & M_{26} & & 0 & 0 & 0 & 0 & 0 & 0 \\ & & & \vdots & & & \ddots & & & & \vdots & & \\ 0 & 0 & 0 & 0 & 0 & 0 & & M_{222} & \Omega_c^* & 0 & -\Omega_a & 0 & 0 \\ 0 & 0 & 0 & 0 & 0 & 0 & & \Omega_c & M_{223} & \Omega_a^* & 0 & -\Omega_a & 0 \\ 0 & 0 & 0 & 0 & 0 & 0 & \cdots & 0 & \Omega_a & M_{224} & 0 & 0 & -\Omega_a \\ 0 & 0 & 0 & 0 & 0 & 0 & & -\Omega_a^* & 0 & 0 & M_{225} & \Omega_c^* & 0 \\ 0 & 0 & 0 & 0 & 0 & 0 & & 0 & -\Omega_a^* & 0 & \Omega_c & M_{226} & \Omega_a^* \\ 0 & 0 & 0 & 0 & 0 & 0 & & 0 & 0 & -\Omega_a^* & 0 & \Omega_a & M_{227} \end{pmatrix}$$

$$\times \begin{bmatrix} a_{22,21}^{(3)} \\ a_{22,31}^{(3)} \\ a_{22,41}^{(3)} \\ a_{23,21}^{(3)} \\ a_{23,31}^{(3)} \\ a_{23,41}^{(3)} \\ \vdots \\ a_{43,21}^{(3)} \\ a_{43,31}^{(3)} \\ a_{43,41}^{(3)} \\ a_{44,21}^{(3)} \\ a_{44,31}^{(3)} \\ a_{44,41}^{(3)} \end{bmatrix} + \begin{bmatrix} -i\Gamma_{21}a_{21}^{(3)} \\ a_{22}^{(2)}-i\Gamma_{21}a_{31}^{(3)} \\ -i\Gamma_{21}a_{41}^{(3)} \\ -a_{21,21}^{(2)} \\ a_{23}^{(2)}-a_{21,31}^{(2)} \\ -a_{21,41}^{(2)} \\ \vdots \\ -a_{41,21}^{(2)} \\ a_{43}^{(2)}-a_{41,31}^{(2)} \\ -a_{41,41}^{(2)} \\ 0 \\ a_{44}^{(2)} \\ 0 \end{bmatrix}, \tag{B5}$$

where $M_{21} = d_{21} + i\Gamma_{21}$, $M_{22} = d_{31} + i\Gamma_{21}$, $M_{23} = d_{41} + i\Gamma_{21}$, $M_{24} = d_{23} + d_{21}$, $M_{25} = d_{23} + d_{31}$, $M_{26} = d_{23} + d_{41}$, $M_{222} = d_{43} + d_{21}$, $M_{223} = d_{43} + d_{31}$, $M_{224} = d_{43} + d_{41} - V$, $M_{225} = d_{21} + i\Gamma_{34}$, $M_{226} = d_{31} + i\Gamma_{34}$, and $M_{227} = d_{41} + i\Gamma_{34} - V$. The initial conditions are given by $a^{(3)}_{33,31}(0) = a^{(2)}_{33}(0)a^{(1)}_{31}(0)$, and other $a^{(3)}_{jl,\mu 1}(0) = 0$. With the solutions obtained at the second-order approximation, solutions of these equations also can be found analytically.

With the results obtained above, we can proceed to the equations of the one-body correlators at the third-order approximation, $\rho^{(3)}_{j1} = a^{(3)}_{j1}|\Omega_p{}^{(1)}|^2\Omega_p{}^{(1)}$ $(j = 2, 3, 4)$, which are given by

$$-i\frac{\partial}{\partial t_0}\begin{bmatrix} a^{(3)}_{21} \\ a^{(3)}_{31} \\ a^{(3)}_{41} \end{bmatrix} = \begin{bmatrix} d_{21} & \Omega_c^* & 0 \\ \Omega_c & d_{31} & \Omega_a^* \\ 0 & \Omega_a & d_{41} \end{bmatrix}\begin{bmatrix} a^{(3)}_{21} \\ a^{(3)}_{31} \\ a^{(3)}_{41} \end{bmatrix} + \frac{i}{\left|\Omega_p{}^{(1)}\right|^2}\frac{\partial}{\partial t_2}\begin{bmatrix} a^{(1)}_{21} \\ a^{(1)}_{31} \\ a^{(1)}_{41} \end{bmatrix} + \begin{bmatrix} a^{(2)}_{23} \\ a^{(2)}_{11} - a^{(2)}_{33} \\ -a^{(2)}_{43} - N_a\int d^3\mathbf{r}' V(\mathbf{r}' - \mathbf{r})a^{(3)}_{44,41} \end{bmatrix}, \tag{B6}$$

where $a^{(3)}_{31} \equiv a^{(3),\mathrm{LA}}_{31} + N_a\int d^3\mathbf{r}' V(\mathbf{r}' - \mathbf{r})a^{(3),\mathrm{RR}}_{31}$, with $a^{(3),\mathrm{LA}}_{31}(0) = 4\gamma_{31}/(\Gamma_{13}|d_{31}|^2)$ and $a^{(3),\mathrm{LA}}_{21}(0) = a^{(4),\mathrm{LA}}_{41}(0) = a^{(3),\mathrm{RR}}_{21}(0) = a^{(3),\mathrm{RR}}_{31}(0) = a^{(3),\mathrm{RR}}_{41}(0) = a^{(3),\mathrm{RR}}_{41}(0)$.

Fourth-order approximation: The first set of equations governing the two-body correlators $\rho^{(4)}_{j1,l1} = a^{(4)}_{j1,l1}|\Omega_p{}^{(1)}|^4$ $(j, l = 2, 3, 4)$ is given by

$$\begin{aligned} -i\frac{\partial}{\partial t_0}\begin{bmatrix} a^{(4)}_{21,21} \\ a^{(4)}_{21,31} \\ a^{(4)}_{21,41} \\ a^{(4)}_{31,31} \\ a^{(4)}_{31,41} \\ a^{(4)}_{41,41} \end{bmatrix} &= \begin{bmatrix} 2d_{21} & 2\Omega_c^* & 0 & 0 & 0 & 0 \\ \Omega_c & d_{21} + d_{31} & \Omega_a^* & \Omega_c^* & 0 & 0 \\ 0 & \Omega_a & d_{21} + d_{41} & 0 & \Omega_c^* & 0 \\ 0 & 2\Omega_c & 0 & 2d_{31} & 2\Omega_a^* & 0 \\ 0 & 0 & \Omega_c & \Omega_a & d_{31} + d_{41} & \Omega_a^* \\ 0 & 0 & 0 & 0 & 2\Omega_a & 2d_{41} - V \end{bmatrix}\begin{bmatrix} a^{(4)}_{21,21} \\ a^{(4)}_{21,31} \\ a^{(4)}_{21,41} \\ a^{(4)}_{31,31} \\ a^{(4)}_{31,41} \\ a^{(4)}_{41,41} \end{bmatrix} \\ &+ \frac{i}{\left|\Omega_p{}^{(1)}\right|^2}\frac{\partial}{\partial t_2}\begin{bmatrix} a^{(2)}_{21,21} \\ a^{(2)}_{21,31} \\ a^{(2)}_{21,41} \\ a^{(2)}_{31,31} \\ a^{(2)}_{31,41} \\ a^{(2)}_{41,41} \end{bmatrix} + \begin{bmatrix} -2a^{(3)}_{23,21} \\ a^{(3)}_{21} - a^{(3)}_{22,21} - 2a^{(3)}_{33,21} - a^{(3)}_{23,31} - a^{(3)}_{44,21} \\ -a^{(3)}_{23,41} - a^{(3)}_{43,21} \\ 2a^{(3)}_{31} - 2a^{(3)}_{22,31} - 4a^{(3)}_{33,31} - a^{(3)}_{44,31} \\ a^{(3)}_{41} - a^{(3)}_{22,41} - a^{(3)}_{44,41} - a^{(3)}_{43,31} \\ -2a^{(3)}_{43,41} \end{bmatrix}. \end{aligned} \tag{B7}$$

The second set of equations governing the two-body correlators $\rho^{(4)}_{j1,1l} = a^{(4)}_{j1,1l}|\Omega_p{}^{(1)}|^4$ $(j, l = 2, 3, 4)$ reads as

$$\begin{aligned} -i\frac{\partial}{\partial t_0}\begin{bmatrix} a^{(4)}_{21,12} \\ a^{(4)}_{21,13} \\ a^{(4)}_{21,14} \\ a^{(4)}_{31,12} \\ a^{(4)}_{31,13} \\ a^{(4)}_{31,14} \\ a^{(4)}_{41,12} \\ a^{(4)}_{41,13} \\ a^{(4)}_{41,14} \end{bmatrix} &= \begin{bmatrix} M_{11} & -\Omega_c & 0 & \Omega_c^* & 0 & 0 & 0 & 0 & 0 \\ -\Omega_c^* & M_{12} & -\Omega_a & 0 & \Omega_c^* & 0 & 0 & 0 & 0 \\ 0 & -\Omega_a^* & M_{13} & 0 & 0 & \Omega_c^* & 0 & 0 & 0 \\ \Omega_c & 0 & 0 & M_{14} & -\Omega_c & 0 & \Omega_a^* & 0 & 0 \\ 0 & \Omega_c & 0 & -\Omega_c^* & M_{15} & -\Omega_a & 0 & \Omega_a^* & 0 \\ 0 & 0 & \Omega_c & 0 & -\Omega_a^* & M_{16} & 0 & 0 & \Omega_a^* \\ 0 & 0 & 0 & \Omega_a & 0 & 0 & M_{17} & -\Omega_c & 0 \\ 0 & 0 & 0 & 0 & \Omega_a & 0 & -\Omega_c^* & M_{18} & -\Omega_a \\ 0 & 0 & 0 & 0 & 0 & \Omega_a & 0 & -\Omega_a^* & M_{19} \end{bmatrix}\begin{bmatrix} a^{(4)}_{21,12} \\ a^{(4)}_{21,13} \\ a^{(4)}_{21,14} \\ a^{(4)}_{31,12} \\ a^{(4)}_{31,13} \\ a^{(4)}_{31,14} \\ a^{(4)}_{41,12} \\ a^{(4)}_{41,13} \\ a^{(4)}_{41,14} \end{bmatrix} + \frac{i}{\left|\Omega_p{}^{(1)}\right|^2}\frac{\partial}{\partial t_2}\begin{bmatrix} a^{(2)}_{21,12} \\ a^{(2)}_{21,13} \\ a^{(2)}_{21,14} \\ a^{(2)}_{31,12} \\ a^{(2)}_{31,13} \\ a^{(2)}_{31,14} \\ a^{(2)}_{41,12} \\ a^{(2)}_{41,13} \\ a^{(2)}_{41,14} \end{bmatrix} \\ &+ \begin{bmatrix} a^{(3)}_{32,21} - a^{(3)*}_{32,21} \\ -a^{(3)*}_{32,31} - a^{(3)}_{21} + 2a^{(3)}_{33,21} + a^{(3)}_{22,21} + a^{(3)}_{44,21} \\ a^{(3)}_{34,21} - a^{(3)*}_{32,41} \\ a^{(3)}_{32,31} + a^{(3)*}_{21} - 2a^{(3)*}_{33,21} - a^{(3)*}_{22,21} - a^{(3)*}_{44,21} \\ -a^{(3)}_{31} + 2a^{(3)}_{33,31} + a^{(3)}_{22,31} + a^{(3)}_{44,31} + a^{(3)*}_{31} - 2a^{(3)*}_{33,31} - a^{(3)*}_{22,31} - a^{(3)*}_{44,31} \\ a^{(3)}_{34,31} + a^{(3)*}_{41} - 2a^{(3)*}_{33,41} - a^{(3)*}_{22,41} - a^{(3)*}_{44,41} \\ a^{(3)}_{32,41} - a^{(3)*}_{34,31} \\ -a^{(3)*}_{34,31} - a^{(3)}_{41} + 2a^{(3)}_{33,41} + a^{(3)}_{22,41} + a^{(3)}_{44,41} \\ a^{(3)}_{34,41} - a^{(3)*}_{34,41} \end{bmatrix}. \end{aligned} \tag{B8}$$

The third set of equations governing the two-body correlators $\rho^{(4)}_{jl,\mu\nu} = a^{(4)}_{jl,\mu\nu}|\Omega_p{}^{(1)}|^4$ $(j, l, \mu, \nu = 2, 3, 4)$ reads as

$$-i\frac{\partial}{\partial t_0}\begin{bmatrix} a^{(4)}_{22,22} \\ a^{(4)}_{22,23} \\ a^{(4)}_{22,24} \\ a^{(4)}_{22,32} \\ a^{(4)}_{22,33} \\ a^{(4)}_{22,34} \\ \vdots \\ a^{(4)}_{44,32} \\ a^{(4)}_{44,33} \\ a^{(4)}_{44,34} \\ a^{(4)}_{44,42} \\ a^{(4)}_{44,43} \\ a^{(4)}_{44,44} \end{bmatrix} = \begin{pmatrix} M_{31} & -2\Omega_c & 0 & 2\Omega_c^* & -2i(\Gamma_{21}+\Gamma_{23}) & 0 & & 0 & 0 & 0 & 0 & 0 & 0 \\ -\Omega_c^* & M_{32} & -\Omega_a & 0 & \Omega_c^* & 0 & & 0 & 0 & 0 & 0 & 0 & 0 \\ 0 & -\Omega_a^* & M_{33} & 0 & 0 & \Omega_c^* & & 0 & 0 & 0 & 0 & 0 & 0 \\ \Omega_c & 0 & 0 & M_{34} & -\Omega_c & 0 & \cdots & i\Gamma_{21} & 0 & 0 & 0 & 0 & 0 \\ 0 & \Omega_c & 0 & -\Omega_c^* & M_{35} & \Omega_a^* & & 0 & i\Gamma_{21} & 0 & 0 & 0 & 0 \\ 0 & 0 & \Omega_c & 0 & -\Omega_a^* & M_{36} & & 0 & 0 & i\Gamma_{21} & 0 & 0 & 0 \\ & & & \vdots & & & \ddots & & & \vdots & & & \\ 0 & 0 & 0 & 0 & 0 & 0 & & M_{340} & -\Omega_c & 0 & \Omega_a^* & 0 & 0 \\ 0 & 0 & 0 & 0 & 0 & 0 & & -\Omega_c^* & M_{341} & \Omega_a & 0 & \Omega_a^* & 0 \\ 0 & 0 & 0 & 0 & 0 & 0 & & 0 & -\Omega_a^* & M_{342} & 0 & 0 & 0 \\ 0 & 0 & 0 & 0 & 0 & 0 & \cdots & \Omega_a & 0 & 0 & M_{343} & -\Omega_c & 0 \\ 0 & 0 & 0 & 0 & 0 & 0 & & 0 & \Omega_a & 0 & -\Omega_c^* & M_{344} & 0 \\ 0 & 0 & 0 & 0 & 0 & 0 & & 0 & 0 & 2\Omega_a & 0 & -2\Omega_a^* & M_{345} \end{pmatrix}$$

$$\times \begin{bmatrix} a^{(4)}_{22,22} \\ a^{(4)}_{22,23} \\ a^{(4)}_{22,24} \\ a^{(4)}_{22,32} \\ a^{(4)}_{22,33} \\ a^{(4)}_{22,34} \\ \vdots \\ a^{(4)}_{44,32} \\ a^{(4)}_{44,33} \\ a^{(4)}_{44,34} \\ a^{(4)}_{44,42} \\ a^{(4)}_{44,43} \\ a^{(4)}_{44,44} \end{bmatrix} + \begin{bmatrix} -2i\Gamma_{21}a^{(4)}_{22} \\ -i\Gamma_{21}a^{(4)}_{23} - a^{(3)}_{22,21} \\ -i\Gamma_{21}a^{(4)}_{24} \\ a^{(3)*}_{22,21} - i\Gamma_{21}a^{(4)}_{32} \\ -i\Gamma_{21}a^{(4)}_{33} - a^{(3)}_{22,31} \\ a^{(3)*}_{22,41} - i\Gamma_{21}a^{(4)}_{34} \\ \vdots \\ a^{(3)}_{44,21} \\ a^{(3)*}_{44,31} - a^{(3)}_{44,31} \\ a^{(3)*}_{44,41} \\ 0 \\ -a^{(3)}_{44,41} \\ 0 \end{bmatrix}, \tag{B9}$$

where $M_{31} = -2i\Gamma_{21}$, $M_{32} = d_{23} + i\Gamma_{21}$, $M_{33} = d_{24} + i\Gamma_{21}$, $M_{34} = d_{32} + i\Gamma_{21}$, $M_{35} = i(\Gamma_{23} + \Gamma_{13} + \Gamma_{21})$, $M_{36} = d_{34} + i\Gamma_{21}$, $M_{340} = d_{32} + i\Gamma_{34}$, $M_{341} = i(\Gamma_{34} + \Gamma_{23} + \Gamma_{13})$, $M_{342} = d_{34} + i\Gamma_{34}$, $M_{343} = d_{42} + i\Gamma_{34} - V$, $M_{344} = d_{43} + i\Gamma_{34} - V$, and $M_{345} = 2i\Gamma_{34}$.

The equation for the one-body correlators $\rho^{(4)}_{jl} = a^{(4)}_{jl}|\Omega_p{}^{(1)}|^4$ $(j, l = 2, 3, 4)$ at this order is

$$-i\frac{\partial}{\partial t_0}\begin{bmatrix} a^{(4)}_{22} \\ a^{(4)}_{33} \\ a^{(4)}_{44} \\ a^{(4)}_{23} \\ a^{(4)}_{24} \\ a^{(4)}_{32} \\ a^{(4)}_{34} \\ a^{(4)}_{42} \\ a^{(4)}_{43} \end{bmatrix} = \begin{bmatrix} i\Gamma_{21} & i\Gamma_{21} - i\Gamma_{23} & i\Gamma_{21} & -\Omega_c & 0 & \Omega_c^* & 0 & 0 & 0 \\ 0 & i\Gamma_3 & -i\Gamma_{34} & \Omega_c & 0 & -\Omega_c^* & -\Omega_a & 0 & \Omega_a^* \\ 0 & 0 & i\Gamma_{34} & 0 & 0 & 0 & \Omega_a & 0 & -\Omega_a^* \\ -\Omega_c^* & \Omega_c^* & 0 & d_{23} & -\Omega_a & 0 & 0 & 0 & 0 \\ 0 & 0 & 0 & -\Omega_a^* & d_{24} & 0 & \Omega_c^* & 0 & 0 \\ \Omega_c & -\Omega_c & 0 & 0 & 0 & d_{32} & 0 & \Omega_a^* & 0 \\ 0 & -\Omega_a^* & \Omega_a^* & 0 & \Omega_c & 0 & d_{34} & 0 & 0 \\ 0 & 0 & 0 & 0 & 0 & \Omega_a & 0 & d_{42} & -\Omega_c \\ 0 & \Omega_a & -\Omega_a & 0 & 0 & 0 & 0 & -\Omega_c^* & d_{43} \end{bmatrix} \begin{bmatrix} a^{(4)}_{22} \\ a^{(4)}_{33} \\ a^{(4)}_{44} \\ a^{(4)}_{23} \\ a^{(4)}_{24} \\ a^{(4)}_{32} \\ a^{(4)}_{34} \\ a^{(4)}_{42} \\ a^{(4)}_{43} \end{bmatrix}$$

$$+\frac{i}{\left|\Omega_p{}^{(1)}\right|^2}\frac{\partial}{\partial t_2}\begin{bmatrix}a_{22}^{(2)}\\ a_{33}^{(2)}\\ a_{44}^{(2)}\\ a_{23}^{(2)}\\ a_{24}^{(2)}\\ a_{32}^{(2)}\\ a_{34}^{(2)}\\ a_{42}^{(2)}\\ a_{43}^{(2)}\end{bmatrix}+\begin{bmatrix}0\\ a_{31}^{(3)*}-a_{31}^{(3)}\\ 0\\ -a_{21}^{(3)}\\ N_a\int d^3\mathbf{r}'V(\mathbf{r}'-\mathbf{r})a_{44,24}^{(4)}\\ a_{21}^{(3)*}\\ a_{41}^{(3)*}-\mathcal{N}_a\int d^3\mathbf{r}'V(\mathbf{r}'-\mathbf{r})a_{44,34}^{(3)}\\ -N_a\int d^3\mathbf{r}'V(\mathbf{r}'-\mathbf{r})a_{44,42}^{(3)}\\ -a_{41}^{(3)}-N_a\int d^3\mathbf{r}'V(\mathbf{r}'-\mathbf{r})a_{44,43}^{(3)}\end{bmatrix}, \tag{B10}$$

Fifth-order approximation: The equation of the one-body correlators $\rho_{j1}^{(5)}=a_{j1}^{(5)}|\Omega_p{}^{(1)}|^4\Omega_p{}^{(1)}$ $(j=2,3,4)$ at this order is

$$-i\frac{\partial}{\partial t_0}\begin{bmatrix}a_{21}^{(5)}\\ a_{31}^{(5)}\\ a_{41}^{(5)}\end{bmatrix}=\begin{bmatrix}d_{21}&\Omega_c^*&0\\ \Omega_c&d_{31}&\Omega_a^*\\ 0&\Omega_a&d_{41}\end{bmatrix}\begin{bmatrix}a_{21}^{(5)}\\ a_{31}^{(5)}\\ a_{41}^{(5)}\end{bmatrix}+\frac{i}{\left|\Omega_p{}^{(1)}\right|^2}\frac{\partial}{\partial t_2}\begin{bmatrix}a_{21}^{(3)}\\ a_{31}^{(3)}\\ a_{41}^{(3)}\end{bmatrix}+\begin{bmatrix}a_{23}^{(4)}\\ a_{11}^{(4)}-a_{33}^{(4)}\\ -a_{43}^{(4)}-N_a\int d^3\mathbf{r}'V(\mathbf{r}'-\mathbf{r})a_{44,41}^{(5)}\end{bmatrix}. \tag{B11}$$

At this order, equations governing the two-body correlators $\rho_{jl,\mu1}^{(5)}=a_{jl,\mu1}^{(5)}|\Omega_p{}^{(1)}|^4\Omega_p{}^{(1)}$ $(j,l,\mu=2,3,4)$ are given by

$$-i\frac{\partial}{\partial t_0}\begin{bmatrix}a_{22,21}^{(5)}\\ a_{22,31}^{(5)}\\ a_{22,41}^{(5)}\\ a_{23,21}^{(5)}\\ a_{23,31}^{(5)}\\ a_{23,41}^{(5)}\\ \vdots\\ a_{43,21}^{(5)}\\ a_{43,31}^{(5)}\\ a_{43,41}^{(5)}\\ a_{44,21}^{(5)}\\ a_{44,31}^{(5)}\\ a_{44,41}^{(5)}\end{bmatrix}=\begin{pmatrix}M_{21}&\Omega_c^*&0&-\Omega_c&0&0&\cdots&0&0&0&i\Gamma_{21}&0&0\\ \Omega_c&M_{22}&\Omega_a^*&0&-\Omega_c&0&&0&0&0&0&i\Gamma_{21}&0\\ 0&\Omega_a&M_{23}&0&0&-\Omega_c&&0&0&0&0&0&i\Gamma_{21}\\ -\Omega_c^*&0&0&M_{24}&\Omega_c^*&0&&0&0&0&0&0&0\\ 0&-\Omega_c^*&0&\Omega_c^*&M_{25}&\Omega_a^*&&0&0&0&0&0&0\\ 0&0&-\Omega_c^*&0&\Omega_a&M_{26}&&0&0&0&0&0&0\\ &&&\vdots&&&\ddots&&&&\vdots&&\\ 0&0&0&0&0&0&&M_{222}&\Omega_c^*&0&-\Omega_a&0&0\\ 0&0&0&0&0&0&&\Omega_c&M_{223}&\Omega_a^*&0&-\Omega_a&0\\ 0&0&0&0&0&0&\cdots&0&\Omega_a&M_{224}&0&0&-\Omega_a\\ 0&0&0&0&0&0&&-\Omega_a^*&0&0&M_{225}&\Omega_c^*&0\\ 0&0&0&0&0&0&&0&-\Omega_a^*&0&\Omega_c&M_{226}&-\Omega_a^*\\ 0&0&0&0&0&0&&0&0&-\Omega_a^*&0&\Omega_a&M_{227}\end{pmatrix}$$

$$\times\begin{bmatrix}a_{22,21}^{(5)}\\ a_{22,31}^{(5)}\\ a_{22,41}^{(5)}\\ a_{23,21}^{(5)}\\ a_{23,31}^{(5)}\\ a_{23,41}^{(5)}\\ \vdots\\ a_{43,21}^{(5)}\\ a_{43,31}^{(5)}\\ a_{43,41}^{(5)}\\ a_{44,21}^{(5)}\\ a_{44,31}^{(5)}\\ a_{44,41}^{(5)}\end{bmatrix}+\frac{i}{\left|\Omega_p{}^{(1)}\right|^2}\frac{\partial}{\partial t_2}\begin{bmatrix}a_{22,21}^{(3)}\\ a_{22,31}^{(3)}\\ a_{22,41}^{(3)}\\ a_{23,21}^{(3)}\\ a_{23,31}^{(3)}\\ a_{23,41}^{(3)}\\ \vdots\\ a_{43,21}^{(3)}\\ a_{43,31}^{(3)}\\ a_{43,41}^{(3)}\\ a_{44,21}^{(3)}\\ a_{44,31}^{(3)}\\ a_{44,41}^{(3)}\end{bmatrix}+-\begin{bmatrix}-a_{32,22}^{(4)*}\\ a_{22}^{(4)}-a_{22,22}^{(4)}-2a_{33,22}^{(4)}-a_{22,44}^{(4)}+i\Gamma_{21}a_{31}^{(5)}\\ -a_{43,22}^{(4)}-i\Gamma_{21}a_{41}^{(5)}\\ -a_{21,21}^{(4)}\\ a_{23}^{(4)}-2a_{23,33}^{(4)}-a_{23,22}^{(4)}-a_{23,44}^{(4)}-a_{21,31}^{(4)}\\ -a_{43,23}^{(4)}-a_{41,21}^{(4)}\\ \vdots\\ -a_{42,23}^{(4)}-a_{41,21}^{(4)}\\ a_{43}^{(4)}-a_{43,22}^{(4)}-2a_{43,33}^{(4)}-a_{43,44}^{(4)}-a_{41,31}^{(4)}\\ -a_{43,43}^{(4)}-a_{41,41}^{(4)}\\ -a_{44,32}^{*(4)}\\ a_{44}^{(4)}-2a_{44,33}^{(4)}-a_{44,22}^{(4)}-a_{44,44}^{(4)}\\ -a_{43,43}^{(4)}\end{bmatrix}, \tag{B12}$$

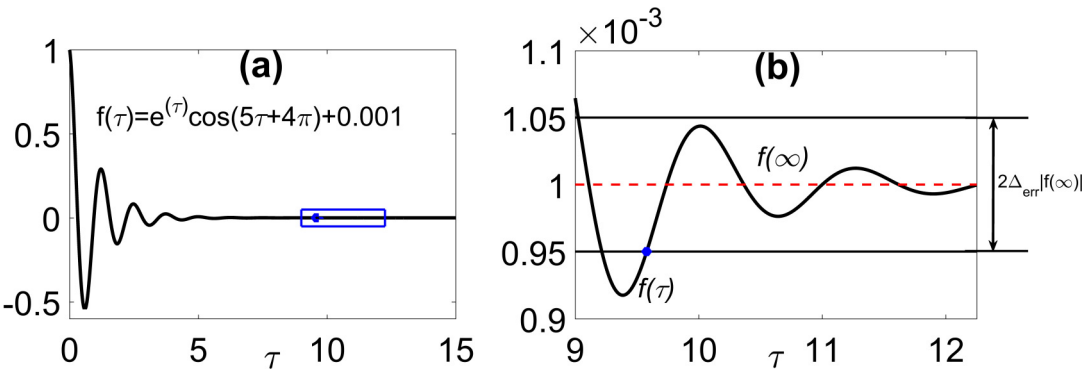

FIG. 7. Definition of the response time of a transient response process, described by a response function $f(\tau)$; τ is dimensionless time. (a) Example: $f(\tau) = e^{-\tau}\cos(5\tau + 4\pi) + 0.001$. The blue rectangle indicates that the variation of $f(\tau)$ reached the range $2\Delta_{\rm err}$ around the steady-state value $f(\infty) = 0.001$. The blue point denotes the response time. (b) Amplification of the blue rectangle shown in (a). The marked region is the error range for defining the response time, bounded by the upper boundary $f(\infty) + |f(\infty)|\Delta_{\rm err}$ and the lower boundary $f(\infty) - |f(\infty)|\Delta_{\rm err}$, with $\Delta_{\rm err} = 0.05$. The blue point is the response time of the transient response process.

where $\rho_{jl,\mu\upsilon} \equiv \langle \hat{S}_{jl}\hat{S}_{\mu\upsilon}\rangle$, $\rho_{j1} = \sum_{m=0}\epsilon^{2m+1}\rho_{j1}^{(2m+1)}$, $\rho_{jl} = \sum_{m=1}\epsilon^{2m}\rho_{jl}^{(2m)}$, $\rho_{11} = 1 + \sum_{m=1}\epsilon^{2m}\rho_{11}^{(2m)}$, $\rho_{j1,l1} = \sum_{m=1}\epsilon^{2m}\rho_{j1,l1}^{(2m)}$, $\rho_{j1,1l} = \sum_{m=1}\epsilon^{2m}\rho_{j1,1l}^{(2m)}$, $\rho_{jl,\mu1} = \sum_{m=1}\epsilon^{2m+1}\rho_{jl,\mu1}^{(2m+1)}$, and $\rho_{jl,\mu\upsilon} = \sum_{m=2}\epsilon^{2m}\rho_{jl,\mu\upsilon}^{(2m)}$ $(j, l, \mu, \upsilon = 2, 3, 4)$.

APPENDIX C: DEFINITION OF THE RESPONSE TIME FOR A TRANSIENT RESPONSE PROCESS

According to the engineering control theory [42], the response time T_R of a transient response process is usually defined to be the minimum time after which the temporal change of the response function describing the transient response process always remains within a small error range $2\Delta_{\rm err} = 0.1$ around the steady-state value of the response. A simple example is shown in Fig. 7, where the normalized response function is $f(\tau) = e^{-\tau}\cos(5\tau + 4\pi) + 0.001$, with τ the dimensionless time. The blue rectangle in Fig. 7(a) means that the variation of $f(\tau)$ has reached the stage where the variation is within the range $2\Delta_{\rm err}|f(\infty)|$ around the steady-state value of the response function, i.e., $f(\infty) = 0.001$. The blue point indicates the position of the response time. Figure 7(b) is the amplification of the blue rectangle shown in Fig. 7(a). The region in green is the permitted relative error range for determining the response time, marked by the upper boundary $f(\infty) + |f(\infty)|\Delta_{\rm err}$ and the lower boundary $f(\infty) - |f(\infty)|\Delta_{\rm err}$. Thus, the blue point is the response time of the transient response process.

[1] M. Fleischhauer, A. Imamoglu, and J. P. Marangos, Electromagnetically induced transparency: Optics in coherent media, Rev. Mod. Phys. **77**, 633 (2005).

[2] *Slow Light: Science and Applications*, edited by K. B. Khurgin and R. S. Tucker (CRC Press, Boca Raton, FL, 2009).

[3] H. Michinel, M. J. Paz-Alonso, and V. M. Perez-Garcia, Turning Light into a Liquid via Atomic Coherence, Phys. Rev. Lett. **96**, 023903 (2006).

[4] A. I. Lvovsky, B. C. Sanders, and W. Tittel, Optical quantum memory, Nat. Photonics **3**, 706 (2009).

[5] R. Santra, E. Arimondo, T. Ido, C. H. Greene, and J. Ye, High-Accuracy Optical Clock via Three-Level Coherence in Neutral Bosonic ^{88}Sr, Phys. Rev. Lett. **94**, 173002 (2005).

[6] T. Zanon-Willette, A. D. Ludlow, S. Blatt, M. M. Boyd, E. Arimondo, and J. Ye, Cancellation of Stark Shifts in Optical Lattice Clocks by Use of Pulsed Raman and Electromagnetically Induced Transparency Techniques, Phys. Rev. Lett. **97**, 233001 (2006).

[7] Y. Wu and L. Deng, Ultraslow Optical Solitons in a Cold Four-State Medium, Phys. Rev. Lett. **93**, 143904 (2004).

[8] G. Huang, L. Deng, and M. G. Payne, Dynamics of ultraslow optical solitons in a cold three-state atomic system, Phys. Rev. E **72**, 016617 (2005).

[9] C. Hang and G. Huang, Weak-light ultraslow vector solitons via electromagnetically induced transparency, Phys. Rev. A **77**, 033830 (2008).

[10] Y. Chen, Z. Bai, and G. Huang, Ultraslow optical solitons and their storage and retrieval in an ultracold ladder-type atomic system, Phys. Rev. A **89**, 023835 (2014).

[11] D. Höckel and O. Benson, Electromagnetically Induced Transparency in Cesium Vapor with Probe Pulses on the Single-Photon Level, Phys. Rev. Lett. **105**, 153605 (2010).

[12] W. R. Anderson, J. R. Veale, and T. F. Gallagher, Resonant Dipole-Dipole Energy Transfer in a Nearly Frozen Rydberg Gas, Phys. Rev. Lett. **80**, 249 (1998).

[13] M. Saffman, T. G. Walker, and K. Mølmer, Quantum information with Rydberg atoms, Rev. Mod. Phys. **82**, 2313 (2010).

[14] O. Firstenberg, C. S. Adams, and S. Hofferberth, Nonlinear quantum optics mediated by Rydberg interactions, J. Phys. B **49**, 152003 (2016).

[15] T. F. Gallagher, *Rydberg Atoms* (Cambridge University Press, Cambridge, 2008).

[16] I. Friedler, D. Petrosyan, M. Fleischhauer, and G. Kurizki, Long-range interactions and entanglement of slow single-photon pulses, Phys. Rev. A **72**, 043803 (2005).

[17] A. K. Mohapatra, T. R. Jackson, and C. S. Adams, Coherent Optical Detection of Highly Excited Rydberg States Using Electromagnetically Induced Transparency, Phys. Rev. Lett. **98**, 113003 (2007).

[18] A. V. Gorshkov, J. Otterbach, M. Fleischhauer, T. Pohl, and M. D. Lukin, Photon-Photon Interactions via Rydberg Blockade, Phys. Rev. Lett. **107**, 133602 (2011).

[19] R. Löw, H. Weimer, J. Nipper, J. B. Balewski, B. Butscher, H. P. Büchler, and T. Pfau, An experimental and theoretical guide to strongly interacting Rydberg gases, J. Phys. B **45**, 113001(2012).

[20] M. Mack, F. Karlewski, H. Hattermann, S. Höckh, F. Jessen, D. Cano, and J. Fortágh, Measurement of absolute transition frequencies of ^{87}Rb to *nS* and *nD* Rydberg states by means of electromagnetically induced transparency, Phys. Rev. A **83**, 052515 (2011).

[21] D. Paredes-Barato and C. S. Adams, All-Optical Quantum Information Processing Using Rydberg Gates, Phys. Rev. Lett. **112**, 040501 (2014).

[22] S. Baur, D. Tiarks, G. Rempe, and S. Dürr, Single-Photon Switch Based on Rydberg Blockade, Phys. Rev. Lett. **112**, 073901 (2014).

[23] H. Gorniaczyk, C. Tresp, J. Schmidt, H. Fedder, and S. Hofferberth, Single-Photon Transistor Mediated by Interstate Rydberg Interactions, Phys. Rev. Lett. **113**, 053601 (2014).

[24] L. Li and A. Kuzmich, Quantum memory with strong and controllable Rydberg-level interactions, Nat. Commun. **7**, 13618 (2016).

[25] M. Marcuzzi, E. Levi, S. Diehl, J. P. Garrahan, and I. Lesanovsky, Universal Nonequilibrium Properties of Dissipative Rydberg Gases, Phys. Rev. Lett. **113**, 210401 (2014).

[26] Q. Zhang, Z. Y. Bai, and G. X. Huang, Fast-responding property of electromagnetically induced transparency in Rydberg atoms, Phys. Rev. A **97**, 043821 (2018).

[27] D. Yan, C. Cui, Y. Liu, L. Song, and J. H. Wu, Normal and abnormal nonlinear electromagnetically induced transparency due to dipole blockade of Rydberg excitation, Phys. Rev. A **87**, 023827 (2013).

[28] J. Stanojevic, V. Parigi, E. Bimbard, A. Ourjoumtsev, and P. Grangier, Dispersive optical nonlinearities in a Rydberg electromagnetically-induced-transparency medium, Phys. Rev. A **88**, 053845 (2013).

[29] C. S. Hofmann, G. Günter, H. Schempp, M. Robert-de-Saint-Vincent, M. Gärttner, J. Evers, S. Whitlock, and M. Weidemüller, Sub-Poissonian Statistics of Rydberg-Interacting Dark-State Polaritons, Phys. Rev. Lett. **110**, 203601 (2013).

[30] V. Parigi, E. Bimbard, J. Stanojevic, A. J. Hilliard, F. Nogrette, R. Tualle-Brouri, A. Ourjoumtsev, and P. Grangier, Observation and Measurement of Interaction-Induced Dispersive Optical Nonlinearities in an Ensemble of Cold Rydberg Atoms, Phys. Rev. Lett. **109**, 233602 (2012).

[31] J. D. Pritchard, A. Gauguet, K. J. Weatherill, and C. S. Adams, Optical non-linearity in a dynamical Rydberg gas, J. Phys. B **44**, 184019 (2011).

[32] S. Sevincli, N. Henkel, C. Ates, and T. Pohl, Nonlocal Nonlinear Optics in Cold Rydberg Gases, Phys. Rev. Lett. **107**, 153001 (2011).

[33] Z. Bai and G. Huang, Enhanced third-order and fifth-order Kerr nonlinearities in a cold atomic system via Rydberg-Rydberg interaction, Opt. Exp. **24**, 4442 (2016).

[34] C. Murray and T. Pohl, Quantum and nonlinear optics in strongly interacting atomic ensembles, *Advances in Atomic, Molecular, and Optical Physics* (Academic, New York, 2016), Vol. 65, Chap. 7.

[35] W. Demtröder, *Laser Spectroscopy: Basic Concepts and Instrumentation*, 3rd ed. (Springer, Berlin, 2003), Chap. 10.

[36] D. Petrosyan, J. Otterbach, and M. Fleischhauer, Electromagnetically Induced Transparency with Rydberg Atoms, Phys. Rev. Lett. **107**, 213601 (2011).

[37] A. Jeffery and T. Kawahawa, *Asymptotic Method in Nonlinear Wave Theory* (Pitman, London, 1982).

[38] A. C. Newell and J. V. Moloney, *Nonlinear Optics* (Addison Wesley, Redwood City, CA, 1992).

[39] J. D. Pritchard, D. Maxwell, A. Gauguet, K. J. Weatherill, M. P. A. Jones, and C. S. Adams, Cooperative Atom-Light Interaction in a Blockaded Rydberg Ensemble, Phys. Rev. Lett. **105**, 193603 (2010).

[40] K. Ogata, *Modern Control Engineering*, 5th ed. (Prentice Hall, Englewood Cliffs, NJ, 2010).

[41] W. S. Levine, *The Control Handbook: Control Systems Fundamentals*, 2nd ed. (CRC Press, Boca Raton, FL, 2011).

[42] H. J. Li, C. Hang, and G. X. Huang, Transient optical properties of coherent four-level atoms without undepleted ground-state approximation, Phys. Lett. A **368**, 336 (2007).